UNCLASSIFIED

AD 258 385

Reproduced
by the

ARMED SERVICES TECHNICAL INFORMATION AGENCY
ARLINGTON HALL STATION
ARLINGTON 12, VIRGINIA
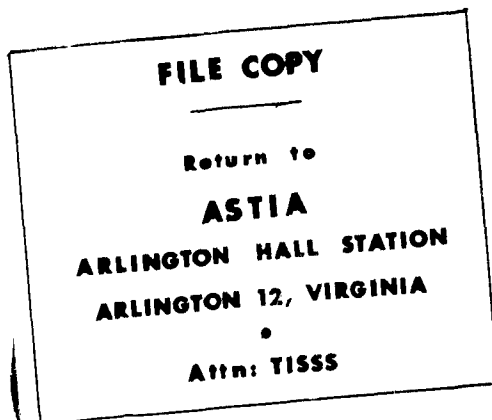
UNCLASSIFIED

75900

only 1 copy
available

61-3-5
XEROX

Contract NBy-3185

Conducted by

ARMOUR RESEARCH FOUNDATION
Chicago, Illinois
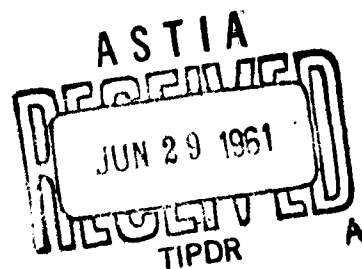
RADIATION STREAMING IN SHELTER ENTRANCEWAYS

October 1960
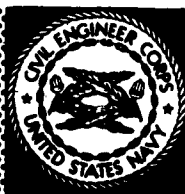
U. S. NAVAL CIVIL ENGINEERING LABORATORY

Port Hueneme, California

$9.10

ARF 1158-12
Final Report

RADIATION STREAMING IN SHELTER ENTRANCEWAYS

Sponsored by:

October 1960

C. W. Terrell (Project Leader)
A. J. Jerri
R. O. Lyday
D. Sperber

ARMOUR RESEARCH FOUNDATION
of
Illinois Institute of Technology
Chicago 16, Illinois

The authors wish to acknowledge the interest and contributions made by others. From Armour Research Foundation, Dr. J. A. Bjorkland for the neutron measurements and W. E. Zagotta for the gamma ray measurements. From the Naval Civil Engineering Laboratory, Capt. A. B. Chilton and Lt. Commander J. C. LeDoux, for their technical suggestions as project monitors.

Work performed on this project is contained in logbooks C-9242, C,-9961, C-9962, C-10330, C-10331, C-10516, and C-10553.

Respectfully submitted,

ARMOUR RESEARCH FOUNDATION
of Illinois Institute of Technology

C.W. Terrell

C. W. Terrell, Supervisor
Reactor Physics Section

APPROVED BY:

J. J. Brophy

J. J. Brophy
Assistant Director of Physics Research

REPORT DISTRIBUTION LIST

No. of Copies	Recipient
1	Chief, Bureau of Yards and Docks Department of the Navy Washington 25, D. C.
1	Dr. Lewis V. Spencer National Bureau of Standards Washington 25, D. C.
1	Mr. John Auxler Oak Ridge National Laboratory Oak Ridge, Tennessee
1	Dr. James O. Buchanan Office of Civil and Defense Mobilization Battle Creek, Michigan
1	Mr. Charles M. Eisenhouer Radiation Physics Laboratory High Voltage Laboratory National Bureau of Standards Washington 25, D. C.
1	Mrs. Shea L. Kruegel, CRTZS Cambridge Research Center Bedford, Massachusetts
1	CAPTAIN William D. Sheehan, U.S.A. Defense Atomic Support Agency Washington 25, D. C.
1	Dr. Ronald Shephard University of California Engineering Field Station 1301 South 46th Street Richmond 4, California
1	Mr. L. Neal FitzSimons Office of Civil and Defense Mobilization Winder Building Washington 25, D. C.
1	Dr. William Kreger U. S. Naval Radiological Defense Laboratory San Francisco 24, California

REPORT DISTRIBUTION LIST

(continued)

No. of Copies	Recipient
1	Mr. Richard Park National Academy of Sciences 2101 Constitution Avenue Washington 25, D. C.
1	Mr. E. E. Shalowitz Protective Construction GSA Building 19th and F Street, N. W. Washington 25, D. C.
1	CAPT A. B. Chilton, CEC, USN U. S. Naval Civil Engineering Laboratory Port Hueneme, California
1	Mr. G. H. Albright The Pennsylvania State University College of Engineering and Architecture University Park, Pennsylvania
1	CDR W. J. Christensen, CEC, USN Bureau of Yards and Docks, Code D-440 Washington 25, D. C.
1	LCDR E. M. Saunders, CEC, USN NROTC Unit Stanford University Palo Alto, California
1	LCDR J. C. LeDoux, CEC, USN U. S. Naval School, CEC Officers Port Hueneme, California
1	Commanding Officer U. S. Chemical Corps Research and Development Command Washington 25, D. C.
1	Chief, Defense Atomic Support Agency Washington 25, D. C.
1	Officer in Charge CECOS (ATTN: ADCE Course) Port Hueneme, California

(continued)

No. of Copies	Recipient
1	Director, Civil Effects Test Group Atomic Energy Commission (ATTN: Mr. R. L. Corsbie) Washington 25, D. C.
1	U. S. Atomic Energy Commission Technical Information Service P. O. Box 62 Oak Ridge, Tennessee
1	Commanding Officer Nuclear Defense Laboratory Army Chemical Center Edgewood, Maryland
1	Commanding Officer and Director Naval Research and Development Laboratory San Francisco, California
1	Technical Operations, Inc. (Contractor) Attn: Dr. Clarke Burlington, Massachusetts
25	Naval Civil Engineering Laboratory Port Hueneme, California
1	ARF Report Library via K. W. Miller
1	ARF Main Files
1	ARF Physics (A) Division Files via Director of Physics Research - L. Reiffel
17	ARF Reactor Physics Section Files
1	Aerojet-General Nucleonics P. O. Box 77 San Ramon, California Attn: Stanton T. Friedman

ABSTRACT

The basic objective of the work reported herein is to study, describe and measure the transport of nuclear radiation through air ducts having walls of different materials. Particular emphasis is placed on full scale concrete ducts which are intended for use as underground shelter entranceways and contain a right angle bend.

It is shown that a modified albedo theory will rather accurately describe the transmission of both gammas and neutrons in lead and concrete ducts. Theory is compared with experimental measurements of gamma dose and neutron flux attenuation factors. Neutron number albedo measurements are made and reported.

Work by various theorists and experimenters are included for completeness and comparison. This program rather clearly points out direction future programs should take and the areas in which major emphasis is needed.

TABLE OF CONTENTS

LIST OF ILLUSTRATIONS

LIST OF ILLUSTRATIONS (continued)

LIST OF TABLES

RADIATION STREAMING IN SHELTER ENTRANCEWAYS

I.   INTRODUCTION

In the winter of 1959, the Armour Research Foundation began work on a program designed to develop basic information on the transport of nuclear radiation through ducts and shelter entranceways. The need for such a program is clearly in evidence from the shelter radiation level measurements made during the Teapot and Plumbob test series. The work reported herein is a combined theoretical and experimental program designed to investigate both neutron and gamma ray transport characteristics.

While the basic objective was information necessary for adequate radiation protection design of personnel shelters, it was recognized that because no experimental data existed for full scale entranceways a contribution to the field of radiation transport could be made. Further, the absence of experimental work, in general, adds value to almost any measurements which are made. Various authors have reported analytical receipts which invoke the albedo concept. Numerous calculations of albedos have been reported but the paucity of experimental values renders comparison of theory and experiment virtually impossible in all but a few special cases.

Consequently, this program, though not part of the original planning, attempts to determine experimental albedo values. We were successful only with neutron number albedo, other attempts being frustrated by scattering from undesired surfaces, inadequate sources or detectors, etc.

This report, in addition to describing the work done on this program, attempts to pull together most work done to date of which we have knowledge.

II.   SUMMARY OF PREVIOUS WORK

A.   Analytical

1.   Simon and Clifford[1]

Simon and Clifford present the following expression for the uncollided flux at the end of a straight cylindrical duct from a plane source of strength n_o.

$$\phi_o = \frac{n_o \delta^2}{2\ell^2} \tag{1}$$

where

δ = radius

ℓ = length of duct

n_o = strength in n/cm^2 - sec isotropically in the forward direction.

This formula is valid for ducts where the radius δ is small compared to the length ℓ. The scattered flux from reflections from the walls is given by:

$$\phi_s = \int_o^\ell \frac{N_o}{2\pi r_1^2} \cdot \frac{\delta}{r_1} \cdot \frac{\alpha'}{2\pi r_2^2} \cdot 2\pi \delta dy \tag{2}$$

[1]Simon, A. and Clifford, C. E. "The Attenuation of Neutrons by Air Ducts in Shields." Nuc. Sci. and Engr. 1, 156-166 (1956).

where

$$N_o = \pi \delta^2 m_o \, ,$$ and α' is the reflection coefficient (albedo).

The dose albedo is defined as the ratio of the dose from a surface to the dose impinging upon the surface. If α' is independent of angle, equation (2) reduces to

$$\phi_s = \frac{N_o \alpha' \lambda}{2\pi \ell^2} \int_0^1 \frac{dt}{\left(\lambda + t^2\right)^{3/2} \left(\lambda + (1-t)^2\right)} \qquad (3)$$

where

$$\lambda = \left(\frac{\delta}{\ell}\right)^2 \qquad\qquad t = \frac{y}{\ell}$$

Simon and Clifford at this point enforces their assumption of $\lambda \ll 1$ and approximates the integral as from 0 to 1/2 instead of from 0 to 1. By this technique, the scattered flux reduces to

$$\phi_s \cong \frac{N_o \alpha'}{2\pi \ell^2} \qquad (4)$$

If the albedo is part isotropic (A) and part cosine (B) the total flux becomes:

$$\phi_T = \frac{N_o}{2\pi \ell^2} \left[1 + A\alpha' + B\alpha'\lambda \right] \qquad (5)$$

-3-

It might be noted that the integral in equation (3) can be integrated directly;[2] however, the solution is very long and since the assumption that the albedo does not change with angle is poor, the added value of the direct integration is highly doubtful. The solution shown in equation (4) is probably as good as is justified by the other assumptions used in the derivation.

The dose after a bend is equivalent to two ducts joined at an angle of Θ. The equation for the dose is

$$D_T = \frac{k n_0 \pi \delta^2}{4} \left(\frac{\delta}{l_1}\right)^2 \left(\frac{\delta}{l_2}\right)^2 \alpha' \left(\frac{A + 2B \sin \theta}{\sin \theta}\right) \tag{6}$$

where k is a factor converting flux to dose. The use of an angular dependent albedo in equation (6) increases its accuracy but the assumption of $\lambda \ll 1$ limits its usefulness.

Simon and Clifford also present a single scattering approach for the attenuation of neutrons down a straight duct. They assume isotropic scattering and that the number of neutrons at a point located at a distance x into the wall is the number incident on the surface multiplied by exp $(-\Sigma_t x)$. Their expressions for the scattered flux at a point inside a straight cylindrical duct is:

$$\phi_s = \frac{N_0 \Sigma_s}{4\pi} \int_0^l \int_0^\infty \frac{(x+\delta) e^{-\Sigma_t d} \, dy \, dx}{\left[y^2 + (\delta+x)^2\right]\left[(l-y)^2 + (\delta+x)^2\right]} \tag{7}$$

___

[2] ARF Monthly Report Number 6 of this contract—Integration performed by H. Wilf.

-4-

where

$$d = \frac{x}{\sin\psi_1} + \frac{x}{\sin\psi_2} = \frac{x}{x+\delta}\left\{\sqrt{(x+\delta)^2 + y^2} + \sqrt{(x+\delta)^2 + (\ell-y)^2}\right\} \quad (8)$$

and x = depth into surface, y = distance from source, Σ_s is scattering cross section and Σ_t is the total cross section. The geometry of the problem is shown in Fig. 1.
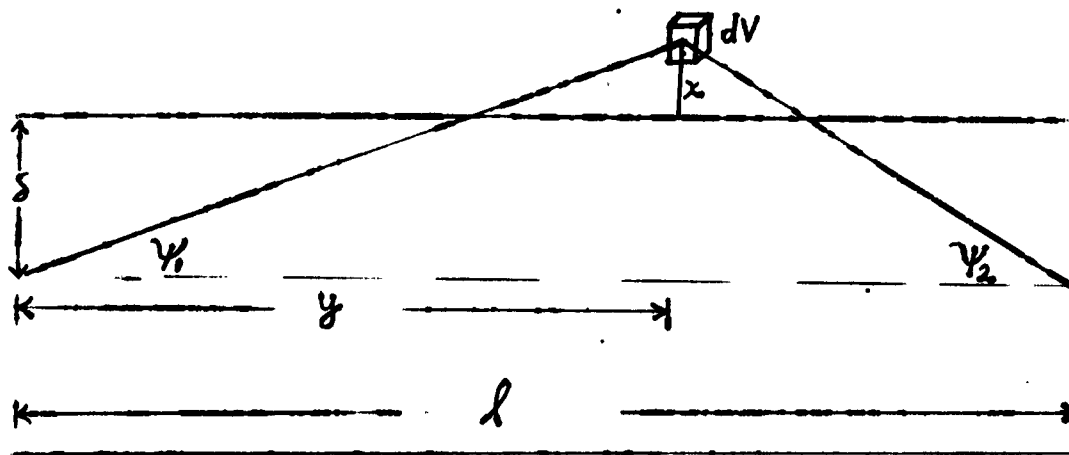
Fig. 1.   Single Scattering Geometry

Since the function under the integral in equation (7) peaks at $x = 0$, all slowly varyfing functions are evaluated at $x = 0$. Setting $\delta/\ell \ll 1$ and $\ell/2\delta \gg 1$ we obtain for the scattered flux

$$\phi_s \cong \frac{N_o \delta}{4\ell^3} \frac{\Sigma_s}{\Sigma_t} \tag{9}$$

This shows that the scattered flux varies as the cube of the length, not as the square as was indicated from the albedo method (see equation (4)). It can be shown that equations (4) and (9) converge when the angular dependent albedo is used in equation (4). The agreement is good for long leg lengths.

Simon and Clifford present also an approximate derivation for multiple reflection which can be summarized in one statement thusly: for a point surrounded by reflecting surfaces, replace the albedo with $\frac{\alpha'}{1-\alpha'}$. This statement involves a good many assumptions and approximations but does yield good results for small δ/ℓ and fair accuracy for δ/ℓ up to $\sim 1/2$. The single scattering technique as outlined by Simon and Clifford will not work very well for gamma rays because of the large energy degradation and high forward scattering.

-6-

2. Roe[3]

Roe treats the streaming problem by a one-group diffusion approach. He uses the same limiting assumption that the radius is small compared to the leg length. Roe does reach a fairly rigorous series solution for very large leg lengths. His results for the scattered flux are:

$$\phi_s \cong \frac{1}{2}(1+\nu)N_o\left(\frac{\delta}{\ell}\right)^2 + \frac{3}{8}(1+\nu)(\nu-1+\frac{4}{\delta\chi})N_o\left(\frac{\delta}{\ell}\right)^3 + ----- \tag{10}$$

where

$$\chi = 3\Sigma_a \Sigma_{tr}$$

$$\lambda = \frac{1}{\Sigma_{tr}}$$

$$\nu = \frac{3K_o(\chi\delta)}{2\lambda\chi K_1(\chi\delta)}$$

ℓ = leg length

δ = duct radius

K_o and K_1 are the standard Bessel functions.

The results are fairly good for large $\frac{\delta}{\ell}$ but suffers from the usual diffusion theory limitations near boundaries.

---

[3] Roe, G. M. "The Penetration of Neutrons Through an Empty Cylindrical Duct in a Shield." KAPL-712 (1952).

3. Barcus [4]

Barcus starts in the same manner as Simon and Clifford, however he uses an integral approach to the problem. He uses the assumption of Simon and Clifford in that the radius is very small as compared to the leg length. The main difference is that the albedo concept is not used.

The expression for the direct flux at point x, which is a distance ℓ away from a plain isotropic source, is

$$\phi_o = \phi \left\{ 1 - \frac{1}{\left[1 + \left(\frac{\delta}{\ell}\right)\right]^{1/2}} \right\}$$

This expression reduces to the Simon and Clifford results if we let $\frac{\delta}{\ell}$ be much less than one. Barcus then derives an expression for the scattered component. He used a Kernel approach with the transport equation. His final expression for the scattered component is:

$$\phi_s = n_o \int P(\theta) \sin \theta d\theta$$

---

[4] Barcus, J. R. "Transmission of Neutrons by Cylindrical Ducts Penetrating Radiation Shields." TID-4500 (14th Ed.) Physics and Mathematics.

where

$$P_{(\theta)} = \frac{C}{4(1-C)} \cdot \frac{(\delta \chi)^2 (\lambda/\delta) \exp\left[-\chi l\left(1+\left(\frac{\delta}{l}\cdot\csc\theta\right)^2 - 2\frac{\delta}{l}\cdot\cot\theta\right)^{\frac{1}{2}}\right]}{\left[1+\left(\frac{\delta}{l}\cdot\csc\theta\right)^2 - 2\frac{\delta}{l}\cdot\cot\theta\right]^{\frac{1}{2}} - (\lambda \chi)(\cos\theta - \frac{\delta}{l}\csc\theta)},$$

(11)

$$\chi\lambda = \tan\frac{\chi\lambda}{C}, \quad C = \frac{\sigma_s}{\sigma_s + \sigma_a}, \text{ and } \lambda = \text{ mean free path}$$

For a $90°$ bend, equation (11) reduces to

$$P_{(90)} = \frac{C}{4(1-C)} \cdot (\chi\delta)^2 (\lambda/l) \frac{\exp\left[-\chi l\left(1+\left(\frac{\delta}{l}\right)^2\right)^{\frac{1}{2}}\right]}{\left[1+\left(\frac{\delta}{l}\right)^2\right]^{\frac{1}{2}} + \frac{\delta}{l}}$$

(12)

and when $\frac{\delta}{l} \ll 1$, we find

$$\phi_s = \frac{n_o}{8} \frac{C}{1-C} \left(\frac{\delta}{l_1}\right)^2 \left(\frac{\delta}{l_2}\right)^2 (\lambda \chi) \exp\left[-\chi l_2\right]$$

(13)

for the scattered flux.

4. <u>LeDoux and Chilton</u>[5]

This work was received as this report was in preparation and as such, no time was available for complete analysis or checking with the work of others. The albedo approach is used with the usual limitation of $\delta/\rho < 1$. Their results appear in the form of four contributing terms:

(a) D_{basic} - radiation scattered from areas A_1, A_2, A_3, and A_4 - utilizing albedo reflection. These areas can see both source and detector.

(b) D_{tr} - radiation scattered from areas A_5, A_6, A_7, and A_8 - utilizing albedo reflection. These are areas where the radiation has passed through the corner.

(c) D_s - corner scattering of radiation which is then directed toward detector.

(d) D_t - direct corner penetration from source to detector.

The rule for inclusion in the solution of the various terms is based on a greater than 10 $^o/o$ effect. Such a cutoff point is taken in order to limit the complexity of the solution.

The summations are performed using average distances and average angles to determine the albedo. Tables are utilized to determine the attenuation ratios for various rectangular geometries.

5 LeDoux, J. C. and Chilton, A. B. "Attenuation of Gamma Radiation Through Two-legged Rectangular Ducts and Shelter Entranceways - An Analytical Approach." Soon to be released under the auspices of the U. S. Naval Civil Engineering Laboratory, Port Heuneme, California.

B. Experimental

As a convenient reference to the reader, we have drawn together that experimental data of which we are aware. The most complete work done is by Eisenhauer[6] at the National Bureau of Standards in which gamma attenuation measurements are made in small concrete ducts. He investigated the "corner effect" by substituting lead for concrete. Unfortunately, his measurements are all made with pocket dosimeters with attendant low accuracy and reproducibility. Figure 2 shows the geometry and his results are presented in Table I. We note that the corner effect is more pronounced in the smaller duct and effects points near the corner most. When a leg length (D) of 68.7 cm is reached the corner effect still contributes 32 ^{o}/o (1.97 mr/hr vs 1.33). This indicates that for small ducts, leakage through and scattering in, the corner has a significant effect on what arrives at the exit of duct. It is shown that this same conclusion holds for full scale entranceways.

Hungerford[7] has collected a series of experimental albedo measurements which attempt to obtain a total albedo for gamma rays and neutrons. Reflection from a flat surface is measured by a detector shielded from the direct source radiation. Hungerford reports values of 0.12 for PoBe neutrons and 0.04 for Co-60 gamma rays in concrete.

---

6   Private communication: Eisenhauer to LeDoux.

7   Hungerford, H. E. "Some Scattering Experiments Performed at the Bulk Shielding Facility." CF-52-4-99, April. 16, 1952 (OTS).
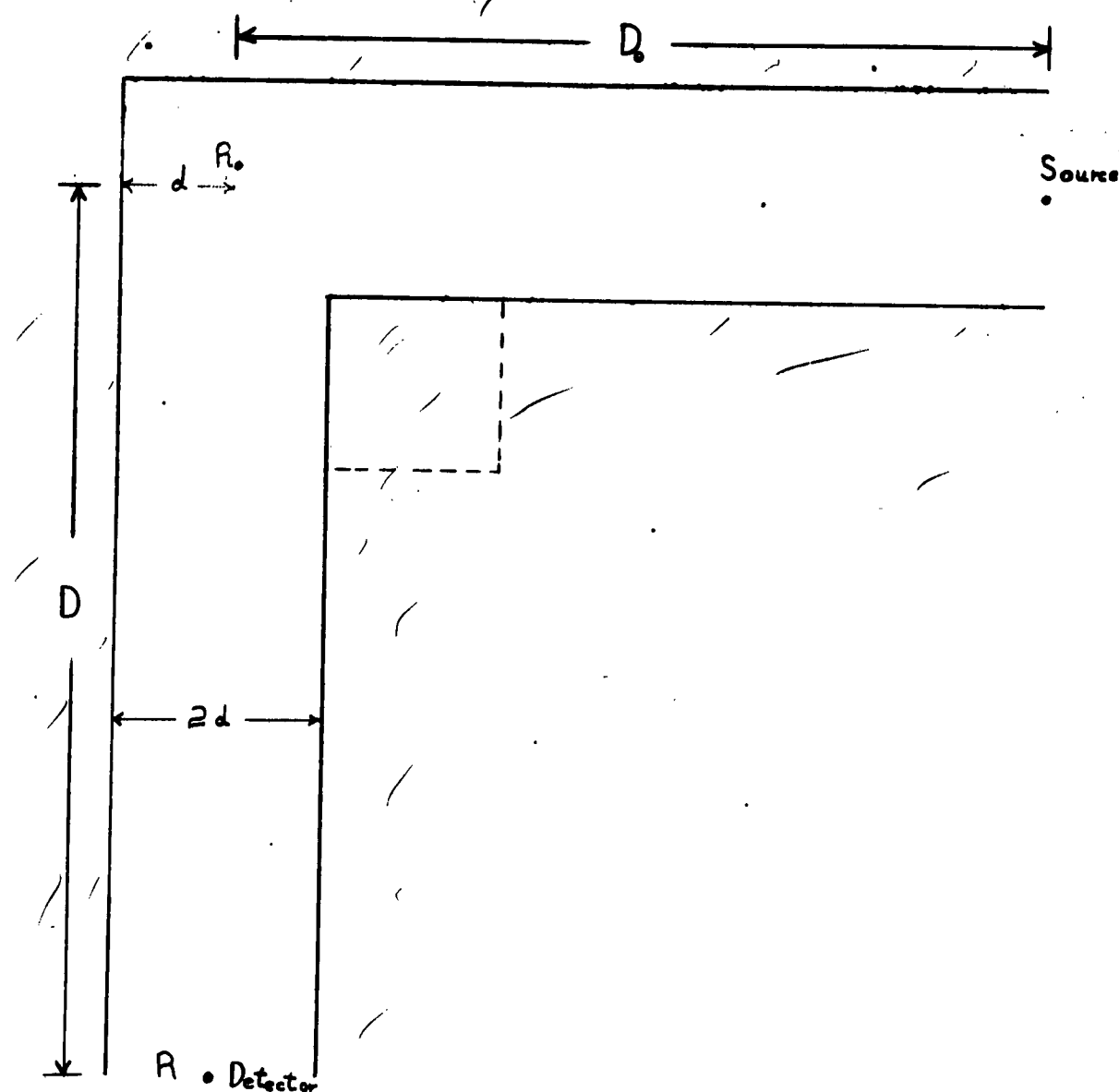
Fig. 2. NATIONAL BUREAU OF STANDARDS
EXPERIMENTAL GEOMETRY FOR
GAMMA ATTENUATION.

Table I

NATIONAL BUREAU OF STANDARDS' CONCRETE AIR DUCT EXPERIMENTAL DATA

D (cm)	d = 9.6 cm			d = 9.6 cm with lead corner			d = 14.1 cm		
	D/d	R(mr/hr)	R/Ro	D/d	R(mr/hr)	R/Ro	D/d	R(mr/hr)	R/Ro
0	0	1080	1.000	0	1080	1.000	0	1050	1.000
14.7	1.53	135	0.125	-	-	-	1.04	934	0.889
18.7	1.95	76.8	0.071	1.95	30.9	0.0286	1.33	-	-
19.7	2.05	67	0.062	2.05	24.4	0.0226	1.40	216	0.206
23.7	2.47	42.8	0.040	2.47	18.8	0.0174	-	-	-
24.7	2.57	39	0.036	-	-	-	1.75	100	0.095
28.7	2.99	26.8	0.0248	2.99	12	0.0111	2.04	68.4	0.065
29.7	3.09	23.5	0.0218	3.09	9.5	0.0080	2.11	64.5	0.061
39.7	4.14	10.3	0.0095	4.14	-	-	2.82	27.6	0.0263
48.7	5.07	5.7	0.0053	5.07	3.3	0.00305	3.45	15.6	0.0148
58.7	6.11	3.15	0.00292	-	-	-	4.16	9.0	0.0086
68.7	7.15	1.97	0.00182	7.15	1.33	0.00123	4.87	5.8	0.0055
78.7	8.20	1.30	0.0012	-	-	-	5.58	3.7	0.0035
88.7	9.24	0.90	0.00083	-	-	-	6.29	2.72	0.0026
98.7	-	-	-	-	-	-	7.00	2.02	0.0019

Work by Cure and Hurst[8] and by Strickler, Gilbert and Auxier[9] using techniques similar to Hungerford report a dose albedo value of 0.32 for PoBe neutrons.

III.   ANALYTICAL PROGRAM

As described earlier, a number of theoretical recipes have been developed to describe the transport of nuclear radiation through straight ducts and through ducts having bends. All of these previous recipes suffer from inherent approximation which seriously limits their applicability. The approximations are in the form of geometry limitations (i. e., $\delta/\ell \ll 1$), energy independence, angular independence, use of diffusion theory, single scattering approximation (dropping of higher order scattering) and others.

Experience with similar problems in reactor theory predicts that use of integral transport theory in which angle and energy dependent scattering is employed would provide a superior recipe. Unfortunately, so many unknowns exist that such an elaborate approach cannot be justified at this time. Similarly, a Monte Carlo approach is not justifiable under this program.

Our approach has been to investigate the more simple treatments with the goal of enhancing their value by suitable correction terms, much in the manner that diffusion theory may be improved by making certain transport corrections.

---

[8] Cure, J. W. and Hurst, G. S. Nucleonics 12, 36-38 (1954).

[9] Strickler, T. D., Gilbert, H. E. and Auxier, J. A. "Fast Neutron Scattering from Slabs, " Nuc. Sci. Engrg. 3, 11-18 (1957).

A. Analytical Methods

The first method investigated is single scattering. The assumption
is made that the dose at a point is due to a direct uncollided flux (D_o) and
to a flux once scattered (D_s) from the walls. The assumption of single
scattering in the walls implies that only the once scattered flux makes a
significant contribution to the dose. In general when $\sigma_s < \sigma_a$ we have a
sufficient condition for the single scattering approximation.

If this is not satisfied one might expect that the amount of
radiation predicted by single scattering will be an underestimate and this was
confirmed by experiment. We therefore have to include a correction due to
multiple scattering. Even double scattering would be very laborious, for all
but the simplest cases, hence, we look for a more phenomenological correction
to single scattering. One way of doing so is to invoke a buildup factor. This
is a number relating the amount of radiation arriving at a certain point, to
that expected if no scattering occurred. The buildup factor is a function of
the number of mean free paths the radiation has traveled in the scattering
material and has the effect of increasing the amount of radiation reaching
the scattering point.

An equivalent method in the case of neutrons is obtained by the
introduction of the removal cross section. This is defined as a measure of
the ability of the material to remove neutrons from a beam.

Another approach is known as the albedo concept. The dose albedo
is defined as the ratio of the dose emerging from a certain point on the
surface, to the dose falling on the surface. The dose and number albedos

-15-

are calculated for gamma rays as a function of energy and angle of incidence. Unfortunately the number albedo for neutrons, which is necessary for the type of neutron detector we employ, is not available. For this reason several experiments are performed and an analysis of the data yields a consistent albedo, which is assumed to be constant over the surface as well as over energy.

1. Single Scattering

We will now present a calculation based on single scattering. We wish to find the radiation at a detector due to a source S; and we will consider two typical detector points: a) points which can see the source (D'), and b) points which get only scattered radiation (D'').
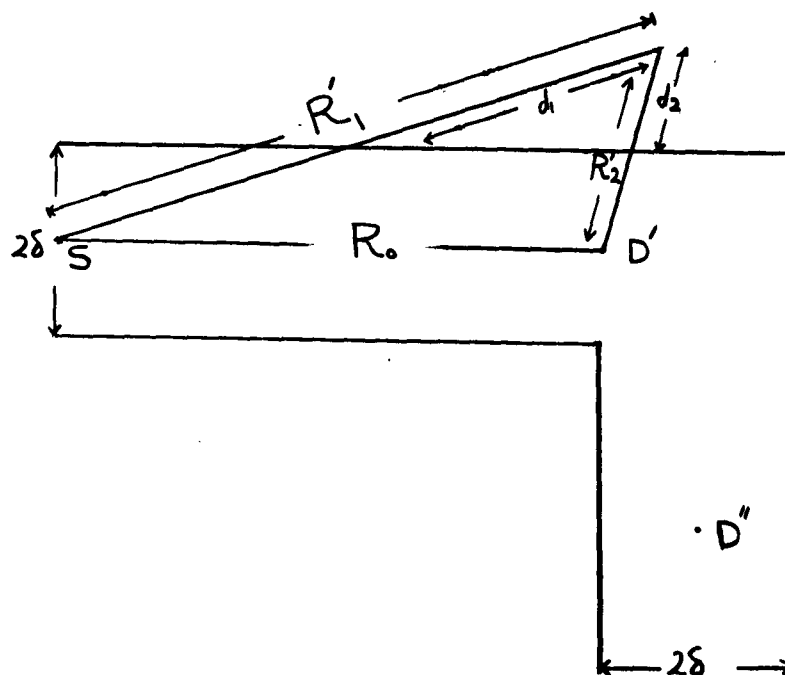
Fig. 3. Single Scattering Geometry

Figure 3 shows a top view of the entranceway. The contribution from a point source to point D' will be

$$D_o = \frac{kS}{4\pi R_o^2} \tag{14}$$

Here S measures the strength of the isotropic point source and k is a conversion factor from flux to dose.

The contribution to the dose at D', from an element of volume dV in the wall, will be:

$$dD_s = \left\{ \frac{kS e^{-\Sigma_t d_1}}{4\pi R_1^2} \Sigma_s \right\} \frac{1}{4\pi R_2^2} e^{-\rho \Sigma_t d_2} dV \tag{15}$$

Here Σ_t is the total cross section for the source energy, $\rho \Sigma_t$ is the same quantity for a flux with degraded energy. Σ_s is the macroscopic scattering cross section which is not necessarily angular independent. The part in the brackets of (15) represents the source per unit volume of the once scattered radiation. To obtain the total contribution due to single scattering one has to integrate over that part of the wall volume which can be seen by the detector. The scattered contribution (D_s) (Σ_s is angularly independent) becomes:

$$D_s = \frac{kS\Sigma_s}{16\pi^2} \iiint \frac{1}{R_1'^2} \cdot \frac{1}{R_2'^2} e^{-\Sigma_t (d_1 + \rho d_2)} dV \tag{16}$$

The volume integration may be reduced to a surface integration
by approximation. From simple geometrical considerations one obtains

$$d_1 = R_1 \frac{x}{x+\delta} \tag{17}$$

$$d_2 = R_2 \frac{x}{x+\delta} \tag{18}$$

The exponential term in the integrand suggests that the main contribution to
the dose at point D' comes from regions where

$$x \ll \delta$$

In this region, all functions except $\frac{x}{x+\delta}$ are slowly varying functions of
x. We therefore can approximate them by their value at $x = 0$. $f(x) = \frac{x}{x+\delta}$
will be approximated by $f(0) + \left(\frac{df}{dx}\right)_{x=0} x$

Hence $\qquad \frac{x}{x+\delta} \sim \frac{x}{\delta}$

Using this simplification the integration over x can be easily carried out.
We obtain:

-18-

$$D_s = \frac{kS}{16\pi^2} \int_V \frac{\Sigma_\delta}{R_1'^2 R_2'^2} \, e^{-\Sigma_t \left(R_1' + PR_2'\right)\frac{x}{x+\delta}} \, dV$$

$$= \frac{kS}{16\pi^2} \Sigma_s \iint \frac{1}{R_1^2 R_2^2} \, e^{-\Sigma_t \left(R_1 + PR_2\right)\frac{x}{x\cdot\delta}} \, dA \, dx$$

$$= \frac{kS}{16\pi^2} \Sigma_s \int \frac{\delta}{R_1^2 R_2^2} \, \frac{dA}{\Sigma_t \left(R_1 + PR_2\right)} \tag{19}$$

The integration is carried out over the area which can be seen from the detector at D'. We therefore get for the total dose D at D'

$$D = \frac{kS}{4\pi} \left[\frac{1}{R_o^2} + \frac{\Sigma_s \delta}{4\pi\Sigma_t} \int \frac{dA}{\left(R_1 + PR_2\right) R_1^2 R_2^2} \right] \tag{20}$$

For a detector placed at a point which cannot see the source, the direct term is eliminated. R_2 and the relevant areas are different in this case, however in every other respect the approach is identical. The integral over the surface area was carried out numerically. The methods of the numerical integration will be explained in a later section.

-19-

2. Build-up Factor Correction to Single Scattering

We shall now see how the build-up factor would effect our single scattering results. The build-up factor is defined as the ratio between the amount of radiation actually arriving at a certain point to that which would be expected should there be no scattering. Scattering builds up radiation at a point because scattering is not a removal process. The amount of radiation arriving at the scattering volume dV is

$$\frac{kS}{4\pi R_1'^2} e^{-\Sigma_t d_1} B(\Sigma_t d_1)$$

where $B(\Sigma_t d_1)$ is the build-up factor and is effective only in the scattering material, not in air. The dose at the detector will be increased again while going through the scattering material and the scattered radiation at D' will be

$$D_s = \frac{kS\Sigma_s}{16\pi^2} \int \frac{e^{-\Sigma_t d_1}}{R_1'^2} \frac{e^{-\rho\Sigma_t d_2}}{R_2'^2} B_1(\Sigma_t d_1) B_2(\rho\Sigma_t d_2) . dV \tag{21}$$

The integration is over all scattering points which can see the detector. The functions B_1 and B_2 are not identical since they include constants which depend on the energy of the scattered radiation as well as the angle of incidence. In the case of gamma rays the build-up factor can well be approximated by

$$B(\Sigma d) = 1 + A (\Sigma d)^{n'} \tag{22}$$

-20-

Here d is the depth the radiation penetrates into the scattering material, A is a constant and n an integer. Both A and n depend on the energy and angle of incidence of the gamma ray. Introducing (22) into (21) we obtain:

$$D_S = \frac{kS\Sigma_s}{16\pi^2} \int \frac{e^{-(\Sigma_t d_1 + \rho \Sigma_t d_2)}}{R_1'^2 \, R_2'^2} \cdot$$

$$\left[1 + A_1(E_1, \varphi_1)(\Sigma_t d_1)^n\right]\left[1 + A_2(E_2, \varphi_2)(\Sigma_t \rho d_2)^n\right] \cdot dV$$

(23)

Making the same approximation as was done for single scattering and elavuating the integral of x from o to ∞ we obtain for the scattered doss

$$D_S = \frac{kS\Sigma_s}{16\pi^2} \int \frac{1}{R_1^2 R_2^2 \left[R_1 + \rho R_2\right]} \left[1 + n! \frac{A_1(E_1, \varphi_1)R_1^n + A_2(\rho E_1, \varphi_2)\rho^n R_2^n}{(R_1 + \rho R_2)^{2n}}\right.$$

$$\left. + \frac{(2n)! R_1^n R_2^n \rho^n}{(R_1 + \rho R_2)^{2n}}\right] dA$$

(24)

The contribution from the direct beam is added to (24). The angle of incidence $\varnothing$ is measured from the vertical.

-21-

3. Albedo Approach

We shall now discuss the albedo method which measures the reflectivity of a medium with respect to an incident flux of radiation. It will generally depend on the kind of radiation under consideration, the manner in which it is applied (number, energy or dose) as well as on the initial condition (energy and angle of incidence). We shall be interested in dose albedos in the case of gamma rays, and in number albedos in the case of neutrons. In the present section a general formula is developed for the albedo approach and for the case where it depends on both the initial energy as well as on the angle of incidence. There will be no difficulty in applying this formula to neutrons for a constant energy albedo.

Let J_+^x be the amount of a certain observable quantity (x will indicate the specific quantity under consideration) falling on a unit area perpendicular to the direction of the beam. Let $J_-^x(\Omega)$ be the same quantity emerging per unit of solid angle. Let ϕ be the angle of incidence. Then we obtain:

$$J_-^x = \alpha(\phi, E) J_+^x f(\Omega) \cos\phi$$

(25)

Equation (25) gives the distribution of the outgoing radiation. If we assume that the outgoing distribution is isotropic we obtain

$$f(\Omega) = \frac{1}{4\pi}$$

(26)

-22-
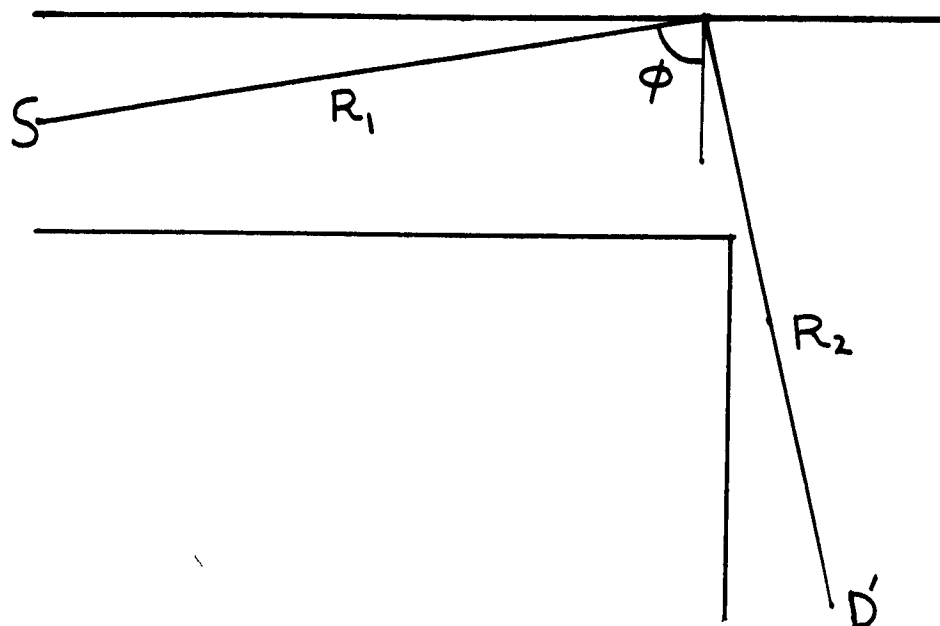
Fig. 4. Albedo Geometry

Figure 4 is again a top view of the entranceway. The source is located at S while the detector is at D'. Using our notation we obtain

$$J_+^x = \frac{kS}{4\pi R_1^2}$$

(27)

Here S measures the strength of the source. Using (25), (26), and (27), we obtain for the scattered dose at D'

$$D_s = \frac{kS}{16\pi^2} \int \frac{\alpha(\phi, E)\cos\phi \, dA}{R_1^2 \, R_2^2}$$

(28)

The manner in which this integration is carried out will be indicated in more detail in a later section treating the methods of integration. There it will also be shown how to take account of multiple reflection whenever it is relevant.

4. The Corner Effect

When comparison is made between experiment and rigorous albedo calculation of the dose distribution in a duct, the agreement is rather poor. Albedo calculations result in lower values than measured. The discrepancy is worse at points just after passing the bend of the entranceway. This suggests that there exists another contribution, which so far has been neglected, and should be incorporated in any calculation. Considering the experimental facts and the geometry it seems quite possible that direct transmission through the corner as well as scattering through the corner is responsible for this discrepancy. We therefore are interested in estimating the possible importance of the corner effect.

The directly transmitted radiation through the corner, which decreases exponentially, is small even for the first position after the bend. We now estimate the value of the scattered component.

Unfortunately, the useful albedo concept is not applicable directly to corner scattering. On the other hand, we know that single scattering gives a considerable underestimate. We now introduce a fictitious albedo to determine the scattered contribution from the corner. We postulate that the ratio between contributions from two different sources (wall and corner) does

-24-

The integration is over the surface of the wall. We shall now perform a similar calculation for the corner.

From Fig. 5. we can see that this contribution will be

$$C_s = \frac{\Sigma_s(\theta)_{corner} kS}{16\pi^2 \Sigma_t^2} \int \frac{e^{-\Sigma_t d_1} e^{-\rho \Sigma_t d_2}}{\pi_1'^2 \, \pi_2'^2} \, dV \tag{31}$$

Here

$$\pi_1'^2 = (x_0 - x)^2 + (y + \delta)^2 + z^2$$

$$\pi_2'^2 = (y_0 - y)^2 + (x + \delta)^2 + z^2$$

$$d_1 = R_1 \frac{y}{y + \delta}$$

$$d_2 = R_2 \frac{x}{x + \delta}$$

and z is a coordinate perpendicular to the drawing. The main contribution will come from volume elements which satisfy

$$x \ll \delta \qquad\qquad y \ll \delta$$

-26-

Fig. 5.   CORNER SINGLE SCATTERING GEOMETRY
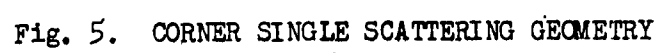
This allows us to follow the approximation developed for single scattering from a wall with the advantage that we can integrate over two coordinates. We obtain

$$C_S = \frac{\Sigma_s(\theta)_{corner}\,\delta^2 k S}{16\pi^2 \rho\, \Sigma_t^2} \int \frac{dz}{\Lambda_1^3 \Lambda_2^3} \tag{32}$$

Here

$$\Lambda_1 = \Lambda_1'(x=0, y=0) = x_0^2 + \delta^2 + z^2$$

$$\Lambda_2 = \Lambda_2'(x=0, y=0) = y_0^2 + \delta^2 + z^2$$

We are left with the integration over one coordinate only. The last integral can be estimated in a similar way to that of equation (30). We obtain

$$C_S = \frac{\Sigma_s(\theta)_{corner}\,\delta^3 k S}{8\pi^2 \rho\, \Sigma_t^2 (\Lambda_1\,\Lambda_2)^3} \tag{33}$$

Using (33) and (30) we obtain for a solution to (29)

$$C_a = \frac{\Sigma_s(\theta)_{corner}(R_1 + \rho R_2) R_1^2 R_2^2}{2\Sigma_t \rho \Lambda_1^3 \Lambda_2^3\, \Sigma_s(\theta)_{wall}} \tag{34}$$

Here (Θ) corner is the average scattering angle for the corner and (Θ) wall is the corresponding quantity for the wall. How this correction term was utilized will be shown in the section discussing numerical methods.

B. Calculated Gamma Ray Albedo Data

The fundamental assumption of earlier gamma ray streaming theories was that the albedo is constant with respect to incident angle. This assumption has been proven false and in fact the angular dependence of the albedo is very large. In obtaining the dose, the need for an angular dependent and energy dependent albedo is deemed entirely necessary. The fundamental source of this data is a report put out by the National Bureau of Standards.[10] Although this report did not give a complete table for variations in angle and energy it did cover the incident angles of $0°$, $30°$, $60°$, and $90°$ (grazing), and energy from 0.2 to 2 mev. The variations in angle and energy permit fairly accurate interpolation and extrapolation for any angle between 0 and $90°$ and any energy between 0.1 and 3 mev. With regard to gamma ray exit angle variation, there is very little data available. The N. B. S. report does mention the variation of the dose with exit angle, but the data is sketchy and only general conclusions can be drawn. The other reference used to find the suitable albedo is by J. F. Perkins[11]. This article has some data on high

10 Berger, M. and D. Raso. "Backscattering of Gamma Rays." N. B. S. Report No. 5982 (July 24, 1958).

11 Perkins, J. F. "Monte Carlo Calculation of Gamma-Ray Albedo of Concrete and Aluminum." Jour. of App. Physics, Vol. 16, No. 4, (June 1955).

energy albedos (0.6 mev to 6 mev). Both sets of data were developed from a
Monte Carlo calculation performed on a computer. N. B. S. used an IBM 704
and Perkins used an IBM 701. The N. B. S. used some 5,000 case histories,
whereas Perkins used only 250 case histories for most of his points. Both
methods took only compton scattering and absorption into account in the compu-
tation of the albedo. Since the angular dependence of the emitted gamma ray
requires more than 5,000 case histories in order to obtain sufficient accuracy,
the emitted gamma distribution was assumed to be isotropic in our calculations.
In particular, the albedo depends on the incident angle, the exit angle, and
the angle between the incident plane and the exit plane as illustrated in Fig. 6.
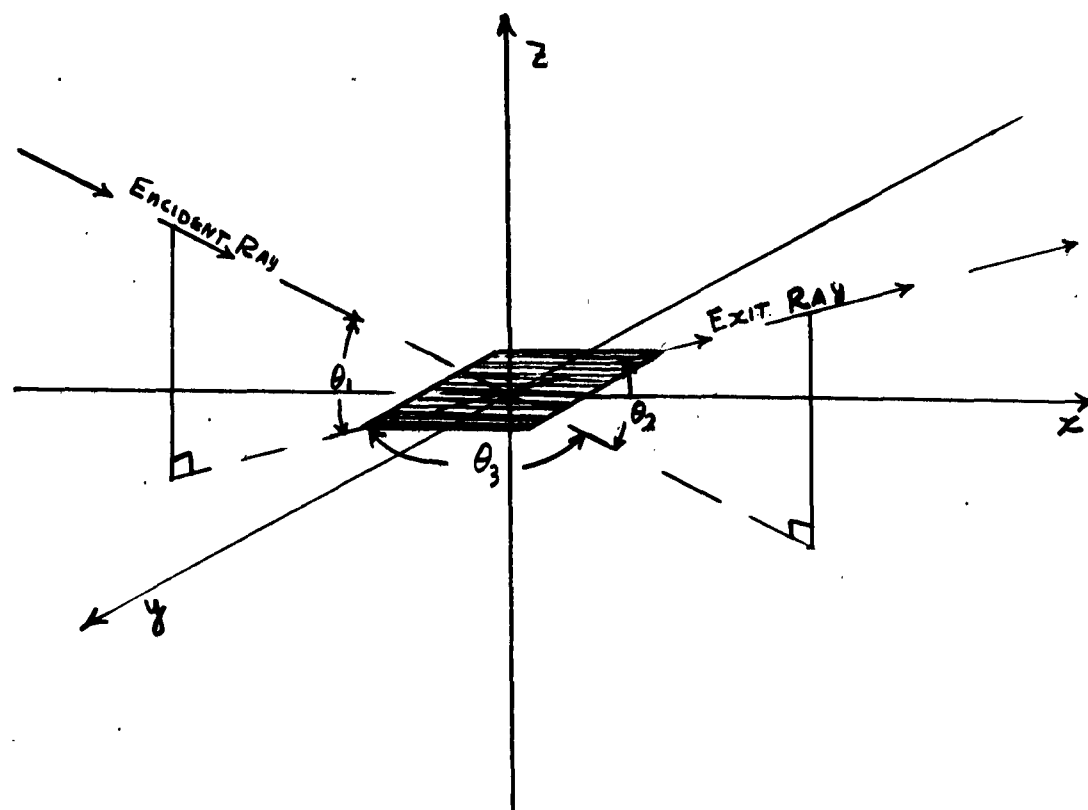
Fig. 6. Albedo Angular Dependence

-30-

Figure 7 shows plots of the various dose albedo data used in the entranceway problem.

C. Numerical Techniques

1. Duct Equations in Rectangular Geometry

As all experimental work is done in rectangular entranceways we present the equations for rectangular geometry.

The expression for single scattering in rectangular geometry is

$$R_1'^2 = (x+\delta)^2 + y^2 + z^2, \quad z = (x+\delta)\tan\psi$$

$$R_2'^2 = (x+\delta)^2 + (\ell-y)^2 + z^2$$

$$d_1 = \frac{x}{\sin\psi_1} = \frac{x}{x+\delta}R_1', \quad d_2 = \frac{x}{\sin\psi_2} = \frac{x}{x+\delta}R_2'$$

$$dV = d(x+\delta)\,dy\,d\left[(x+\delta)\tan\psi\right]$$

So the scattered dose D_s at point D' (Fig. 8) is

$$D_s = \frac{k S \Sigma_s(\theta) P(\theta)}{16\pi^2} \times 4 \times 2 \int_0^\ell \int_0^\infty \int_0^{\pi/4} \frac{dy\,dx\,d\left[(x+\delta)\tan\psi\right]e^{-\Sigma_t d}}{R_1'^2 R_2'^2}$$

-31-
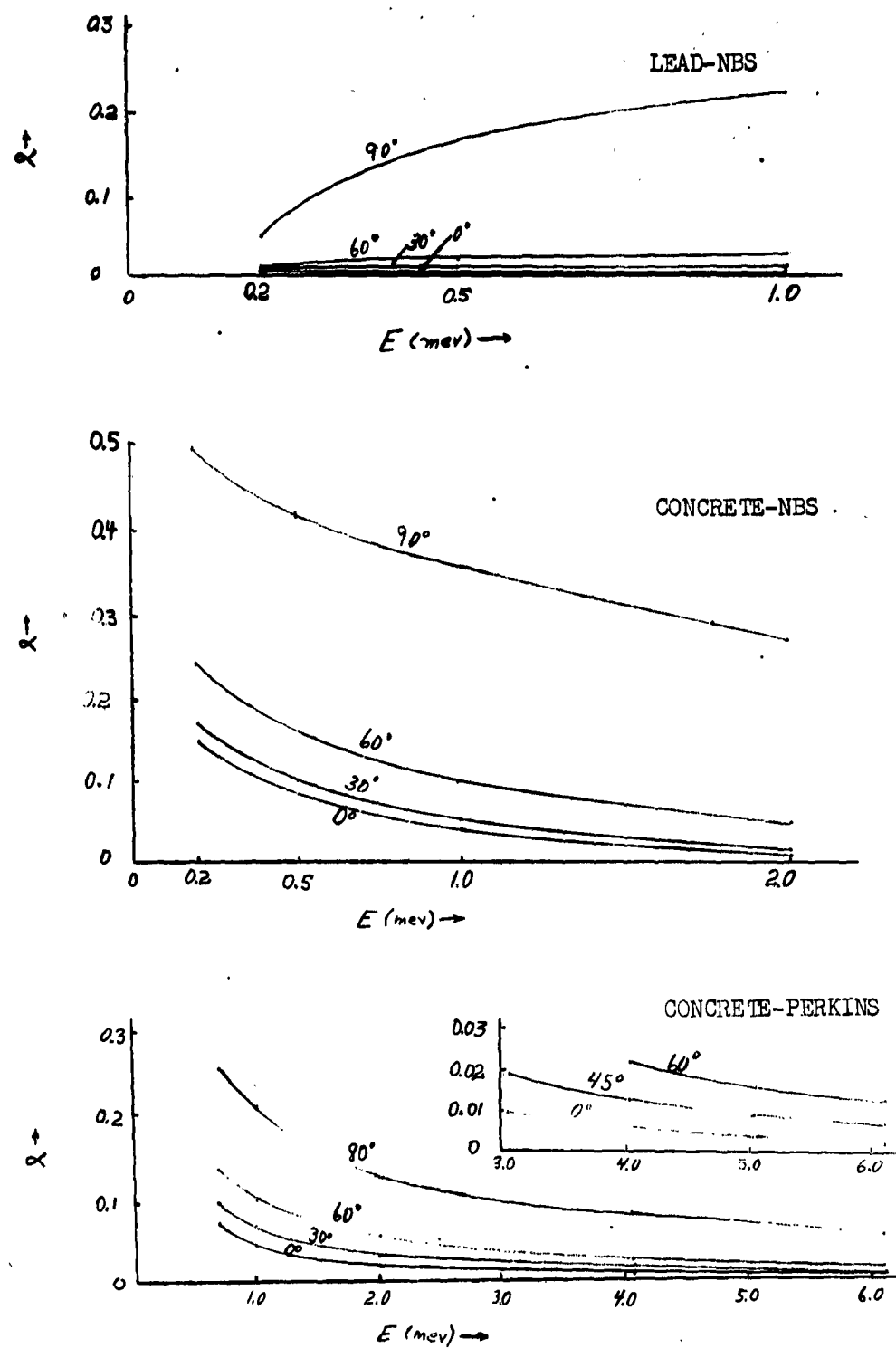
Fig. 7.   CALCULATED GAMMA DOSE ALBEDOS
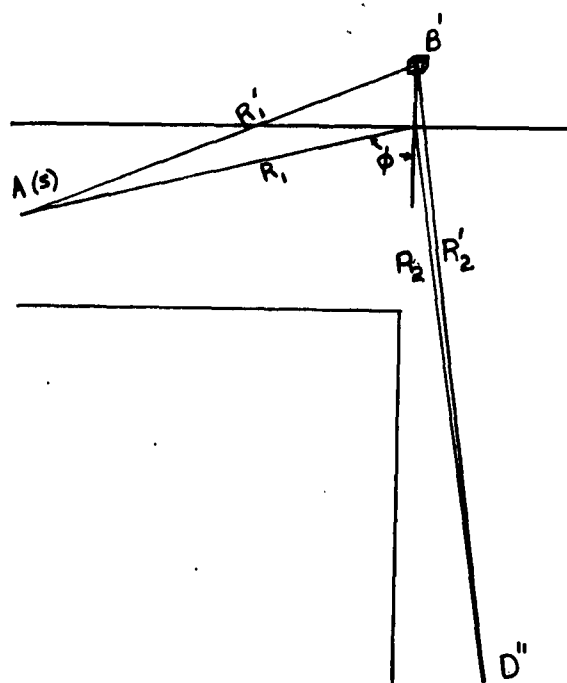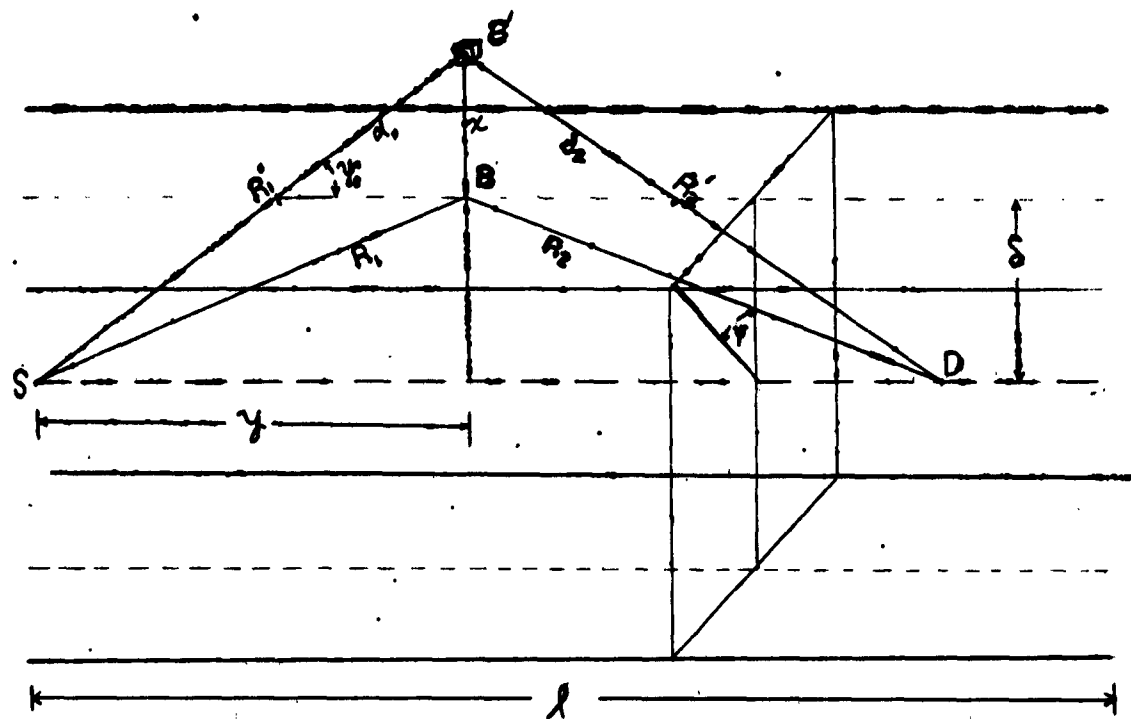
Fig. 8. SINGLE SCATTERING RECTANGULAR GEOMETRY

Carrying the numerical integration for ψ then integrating over x at x = 0 we get

$$D_s = \frac{\delta^2 k S \Sigma_s(\theta) P(\theta)}{2\pi^2} \times 0.9 \int_0^\ell \frac{dy}{R_1^2 R_2^2 \left(\Sigma_t R_1 + \rho \Sigma_t R_2\right)} \tag{35}$$

where the 0.9 factor appears from the integration which will allow us to use $R^2 = \delta^2 + y^2$ instead of $\delta^2 \sec^2\psi + y^2$. Doing the same thing with the cylindrical geometry where there is no need for ψ, we obtain

$$D_s = \frac{\delta^2 k S}{16\pi^2} \Sigma_s(\theta) P(\theta) \times 2\pi \int_0^\ell \frac{dy}{R_1^2 R_2^2 \left(\Sigma_t R_1 + \rho \Sigma_t R_2\right)} \tag{36}$$

When the build-up factor expression $B(\Sigma_t, d) = 1 + A(\Sigma_t d)^n$ is included in the single scattering formula, the final expression in the rectangular geometry will be:

$$D_s = \frac{0.9\delta^2 k S \Sigma_s(\theta) P(\theta)}{2\pi^2 \Sigma_t} \int \frac{dy}{R_1^2 R_2^2 (R_1 + \rho R_2)} \times$$

$$\left\{ 1 + n! \left[A(E_1, \phi_1) R_1^n + \rho^n A(\rho E_1, \phi_2) R_2^n\right] + \frac{(2n)!}{(R_1 + \rho R_2)^{2n}} \left[\rho^n A(E_1, \phi_1) A(\rho E_1, \phi_2) R_1^n R_2^n\right] \right\} \tag{37}$$

-34-

The same thing is done for the wall reflection expression (albedo approach) where we get

$$D_S = \frac{SkS}{8\pi^2} \times 4 \times 2 \times 0.9 \int \frac{\alpha \cos\phi \, \Delta y}{R_1^2 R_2^2}$$

(38)

Here $\alpha = \dfrac{\alpha'}{1-\alpha'}$ to account for the multiple reflection from the four walls.

2. Methods of Numerical Integration

The expression derived above can be numerically integrated along all the wall surface points in the first leg to find the reflected contribution to any point on the centerline of the leg ℓ_1 . In the concrete tunnel Δy was taken to be one foot. R_1 and R_2 are calculated at every point. Also $\alpha(\phi)$ in the case of the albedo approach and $\Sigma_s(\theta)$ and $P(\theta)$ in the case of the single scattering are de mined for each point. In ℓ_1 the four wall scattering surfaces can be considered symmetric with respect to a dose point at the centerline in spite of the ψ angle dependence in our geometry which is taken care of by the factor 0.9. This expression can also be used to calculate the wall reflection contribution to the centerline dose points of the second leg. Dose points in the leg ℓ_2 do not see the source because of the right angle bend, but they receive a reflected contribution from all wall scattering surfaces that can be seen by the dose point and the source at the same time. R_1 and R_2 are calculated from each of these scattering surfaces

to the source and the centerline dose point specified. It should be borne
in mind that only the ceiling and the floor scattering surfaces at the corner
are symmetric with respect to the centerline dose point. $\alpha'(\phi)$, $\sum_s(\theta)$ and
$P(\theta)$ are calculated for each scattering surface also.

In addition to this scattered contribution, dose points
in the second leg and especially those near the corner will receive a con-
tribution from the radiation that falls on the corner and scatters in their
direction. This corner effect is calculated by using single scattering plus
a build-up factor as described previously.

The expression for the corner effect correction that
should be added to the albedo contribution is

$$\frac{C_s}{W_s} = \frac{\sum_s(\theta)_{corner} R_1^2 R_2^2 \left(R_1 + \rho \frac{R_2 \delta}{2\delta + \ell_2}\right)}{\sum_s(\theta)_{Wall} \; 6\rho \eta_1^3 \eta_2^3 \sum_t}$$

It is very important to notice that the reflected contribu-
tion considered here from the points that can be seen by the detector and the
source is a first order reflection which contributes directly to the detector.
A second order reflected contribution can be considered which is due to the first
order reflected radiation being scattered by the second leg walls to the detector.

This is done by considering the first order reflection points as a second order source. This contribution is not going to be important in the case of gamma rays because we are measuring dose which depends on energy and the gamma ray energy after all these reflections has degraded by a large amount. This contribution will be of extreme importance in the case of the neutrons especially when we know that the detector we used is measuring flux per unit time and the albedo we used for this reason is a number albedo. The first order reflection contribution to a centerline point in the second leg is

$$\frac{kS}{8\pi^2} \int \frac{\alpha'}{1-\alpha'} \cdot \frac{\cos\phi}{R_1^2 R_2^2} dA$$

and the flux falling on a unit area of the second leg wall at a distance R_3 (Fig. 9.) from the second order source is

$$\frac{kSdA}{4\pi R_1^2} \cdot \frac{\alpha' \cos\phi}{1-\alpha'} \cdot \frac{\cos\phi'}{2\pi R_3^2} \frac{dA}{1-\alpha'}$$

and the contribution from this point to the detector at a distance R_4 from it is

$$\frac{kSdA}{4\pi R_1^2} \frac{\alpha' \cos\phi}{1-\alpha'} \frac{\cos\phi' dA}{2\pi R_3^2} \frac{\alpha'}{1-\alpha'} \frac{1}{2\pi R_4^2}$$

With x as the corner effect correction factor the total contribution will be

-37-

Fig. 9. GEOMETRY FOR SAMPLE CALCULATION

$$\left[(1+\chi)+R_2^2\int\frac{\alpha'}{1-\alpha'}\ \frac{\cos\phi'dA}{2\pi R_3^2 R_4^2}\right]\cdot\frac{kS}{8\pi^2}\int\frac{\alpha'}{1-\alpha'}\ \frac{\cos\phi\ dA}{R_1^2\ R_2^2}$$

The expression $R_2^2\int\dfrac{\alpha'}{1-\alpha'}\ \dfrac{\cos\phi'dA}{2\pi R_3^2 R_4^2}$ can be related easily to the

integration we did in the first leg. Here the number albedo was chosen to

be constant for different experiments done in concrete and found to be 0.675.

3. Sample Calculations

As an example of the way we did our calculation and numeri-

cal integration the calculation for the dose at position No. 6 is demonstrated

here. As it is shown in Fig. 9., this point is 12 feet from the source. The

source is located two feet from the duct entrance. The source used is a 3.67

curie Co^{60} gamma ray source with 1.59 roentgen per hour per curie at one yard.

The direct dose at this point is

$$1.59 \times (3/12)^2 \times 3.67 \times \frac{1}{60} = 6.032\ mr/min.$$

The reflection contribution will be due to twice the area

of points (1) to (3), four times the area of points (4) to (14), three times

the area from points (15) to (20) and the area from points (21) to (28). At

point 8 for example

$$R_1^2 = 15.25\ ft^2,\ R_2^2 = 99.25\ ft^2,\ \cos\phi = .768, \alpha' = .050,$$

and $\dfrac{\alpha'}{1-\alpha'}\quad \dfrac{\cos\phi}{R_1^2\ R_2^2} = .00002646\ ft^{-4}$

$$\therefore \quad \sum \frac{\alpha'}{1-\alpha'} \frac{\cos\phi}{R_1^2 R_2^2} = 0.00208437$$

but $$\frac{kS}{4\pi} \frac{\delta}{\pi} \times 0.9 = 742.697 \text{ mr/min} \cdot \text{ft}^4$$

$$\therefore \quad \frac{kS}{4\pi} \frac{\delta}{\pi} \times 0.9 \sum \frac{\alpha'}{1-\alpha'} \frac{\cos\phi}{R_1^2 R_2^2} = 742.697 \times .0020844$$

$$= 1.548 \text{ mr/min}$$

The total dose D at position No. 6 is

$$D = 6.032 + 1.548 = 7.58 \text{ mr/min} .$$

The dose without the roof can be calculated by taking the roof contribution which is due to points (15) to (20) from the total reflection contribution which makes it

$$742.697 \times 0.001840 = 1.3666 \text{ mr/min}$$

$$\text{the total dose} = 6.0323 + 1.3584 = 7.499 \text{ mr/min}$$

The same thing will be done to any gamma ray source with only one variable which is the albedo value. In the neutron case the number albedo is taken as a constant as we have no energy or angle dependence.

-40-

IV. EXPERIMENTAL PROGRAM

The experimental part of this program places major emphasis on the measurement of the attenuation in a concrete entranceway. The exact size of the entranceway is chosen to be variable so as to apply to vent ducts as well as personnel entranceways. With these ideas in mind, the entranceway is constructed out of double-interlocking concrete blocks. While these blocks were being obtained, a small duct with a right angle bend was constructed out of lead to check theory and experiment. More work on lead is planned.

A. Description of Experimental Entranceways

1. Lead Duct

The lead duct was constructed of $8" \times 4" \times 2"$ lead bricks. The duct has an $8" \times 8"$ cross section and each leg is 16 " long. A photograph of the duct is shown in Fig. 10. where the roof has been removed in order to see the actual construction in more detail. The walls, floor, and roof have a minimum thickness of four inches of lead. Note that the right angle corner has been filled with more lead brick in order to insure no direct leakage through walls.

2. Concrete Entranceway

The concrete blocks are designed to interlock in two directions so as to prevent leakage through cracks. The blocks were of various sizes and shapes, and range from an 8 foot by 4 foot by 1 foot block to a 1 foot cube. The minimum entranceway size possible with these blocks is a 1 foot by 1 foot
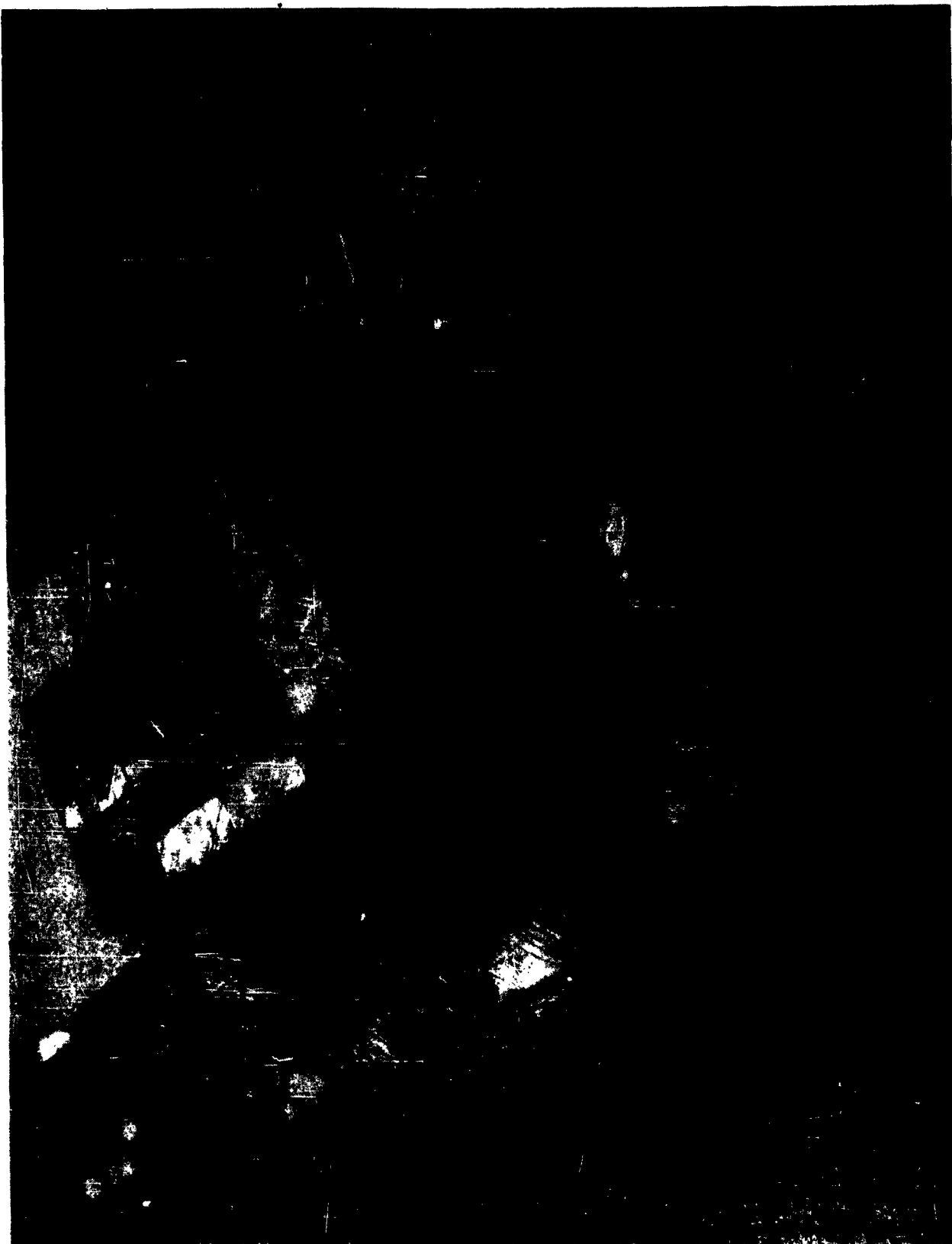
Fig. 10 - LEAD DUCT WITH ROOF REMOVED.

cross section and 1 foot length to a 6 foot cross section and 2 foot length. The maximum leg length is about 30 feet with intermediate cross sections of two and four feet. The cross section does not have to be square, however this simplifies the calculations. The drawings in Fig. 11. show the general construction of the concrete blocks. The blocks that are required are: 1) standard block, 2) starting block, 3) ending block, 4) top block, 5) bottom block, 6) start-top block, 7) start-bottom block, 8) end-top block, and 9) end-bottom block. All blocks are derived from the standard block by passing a plane through the standard·block perpendicular to the flat outside surface as is noted in Fig. 11. All parts of the wall interlock to prevent leakage; however, the top row and the bottom row of blocks are flat to accommodate the roof and floor. The parts of the roof can be seen to interlock in Fig. 12. The roof itself interlocks but not with the wall. Figure 13 shows the concrete entranceway partially assembled with the reactor thermal column door part way out. The entranceway was constructed so that the thermal column door can pass down the entranceway and the reactor used as a neutron (or gamma) source. Figure 14 shows the almost completed entranceway with the right angle section of the roof removed. The right angle roof section that is shown removed is the physical setup used when the data in this report refers to "with roof removed." Figure 15 shows the complete entranceway as it is assembled for the measurements. The composition of the concrete is as follows: To one bag of portland cement, 205 pounds of sand torpedo 1/dry, 240 pounds of 3/4 inch stone chips, and 5 to 5.5 gal. of water. 4,000 psi compressive strength resulted.

TOP

SIDE

(1)

END

STANDARD BLOCK

(3) (2)

(5)

(4)

(9) (7)

(8) (6)
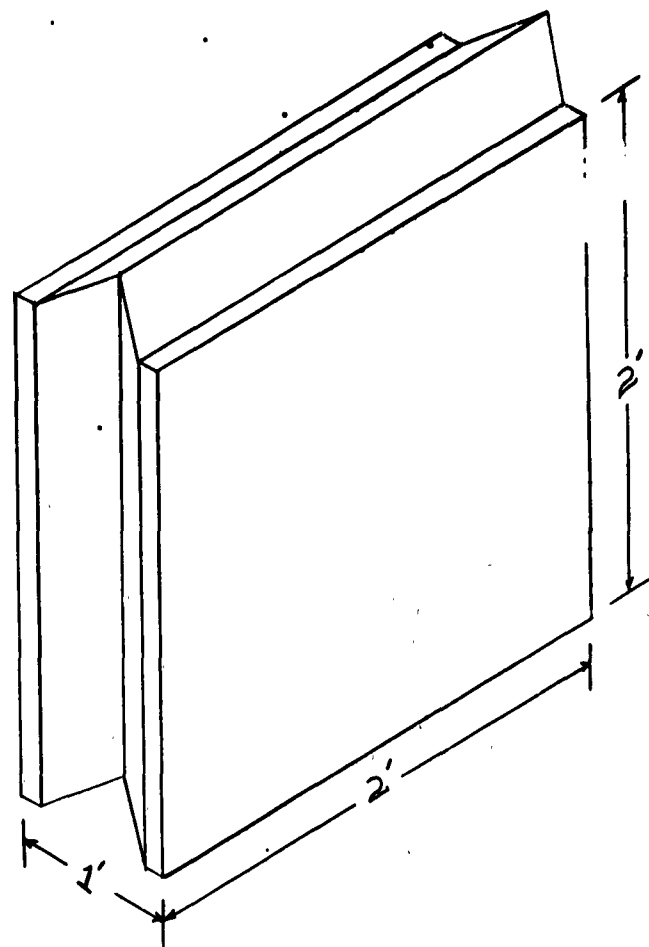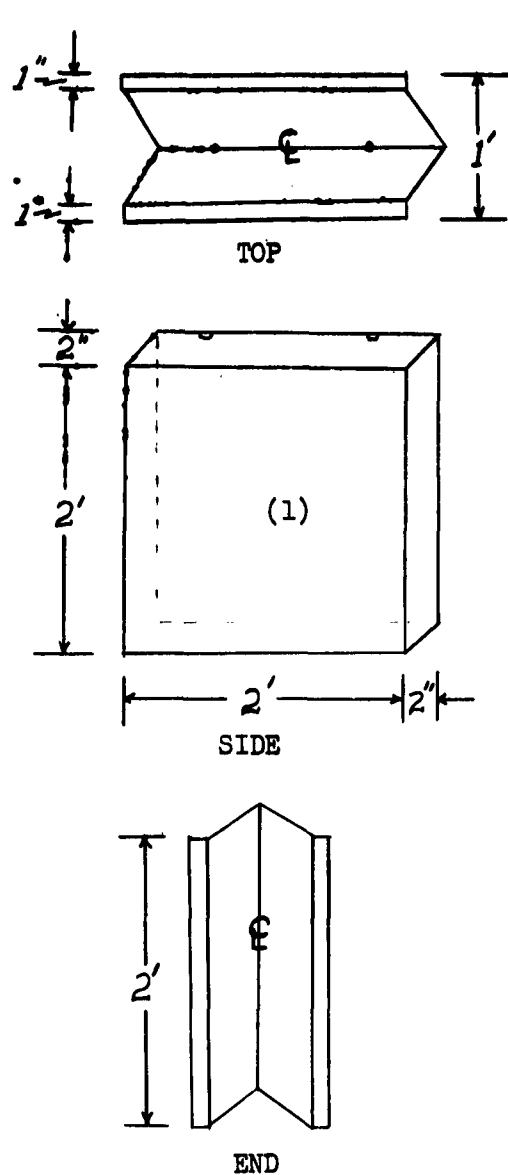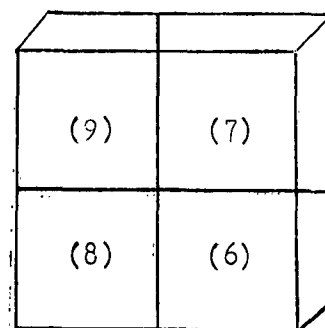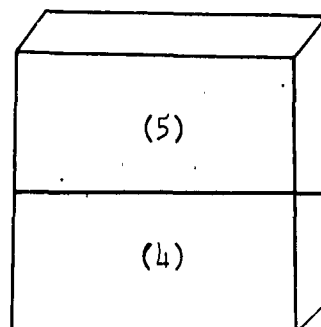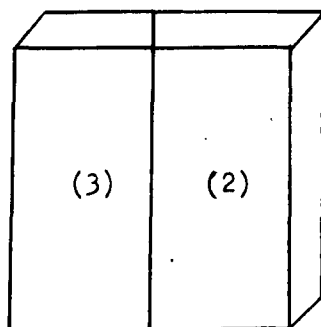
Fig. 11. CONCRETE ENTRANCEWAY BLOCKS
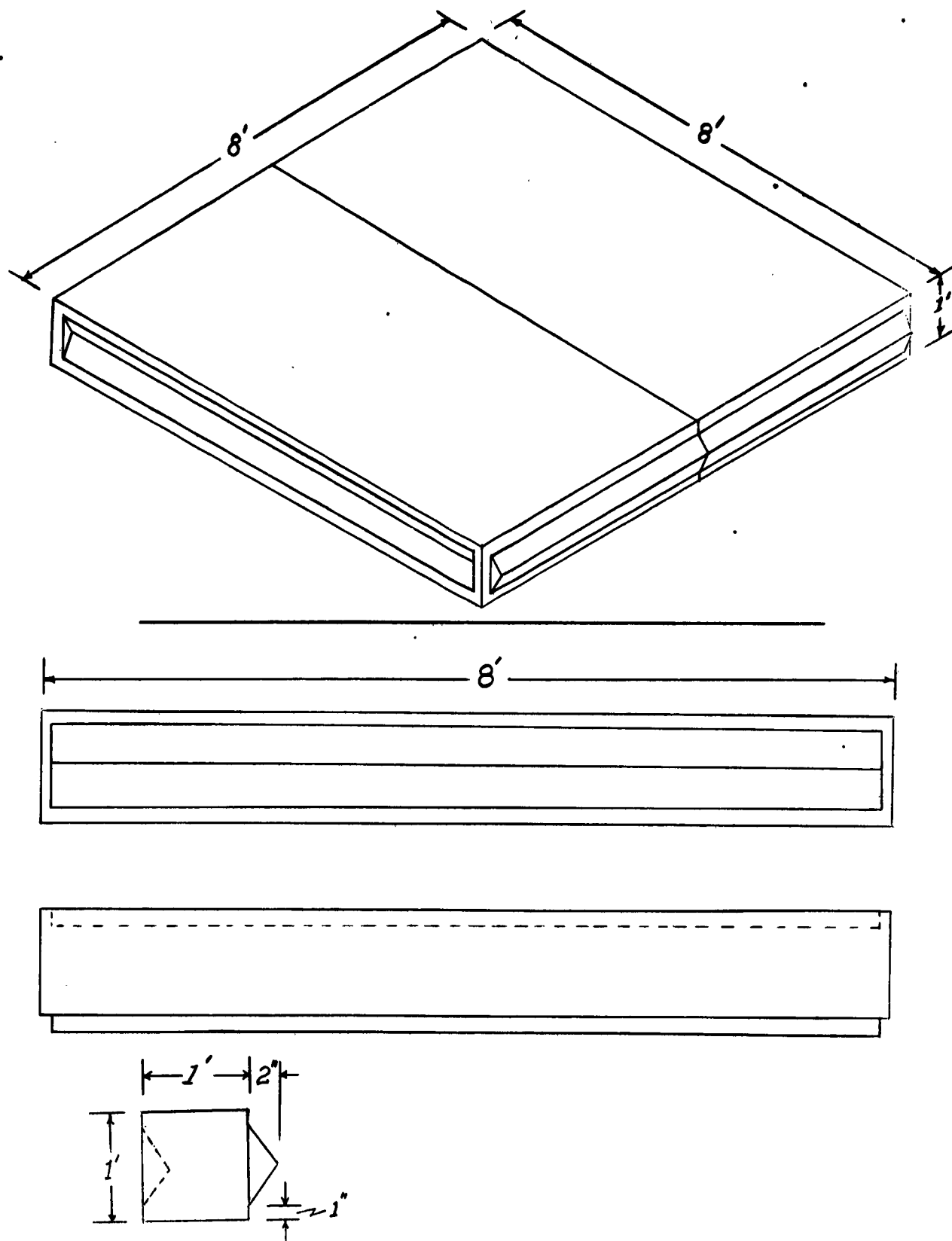
Fig. 12. CONCRETE ENTRANCEWAY CEILING BLOCKS
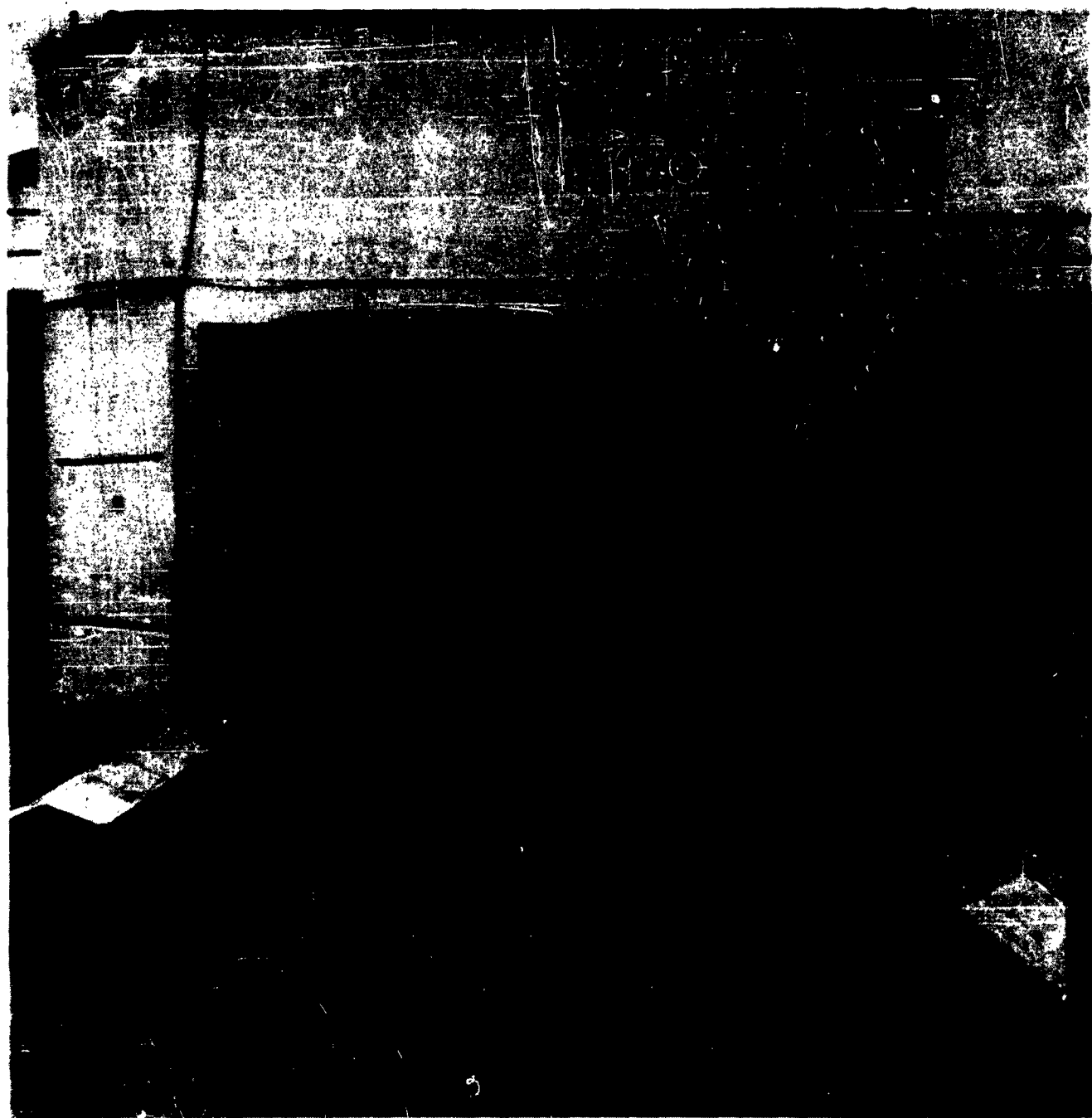
Fig. 13 - CONCRETE ENTRANCEWAY PARTIALLY ASSEMBLED.
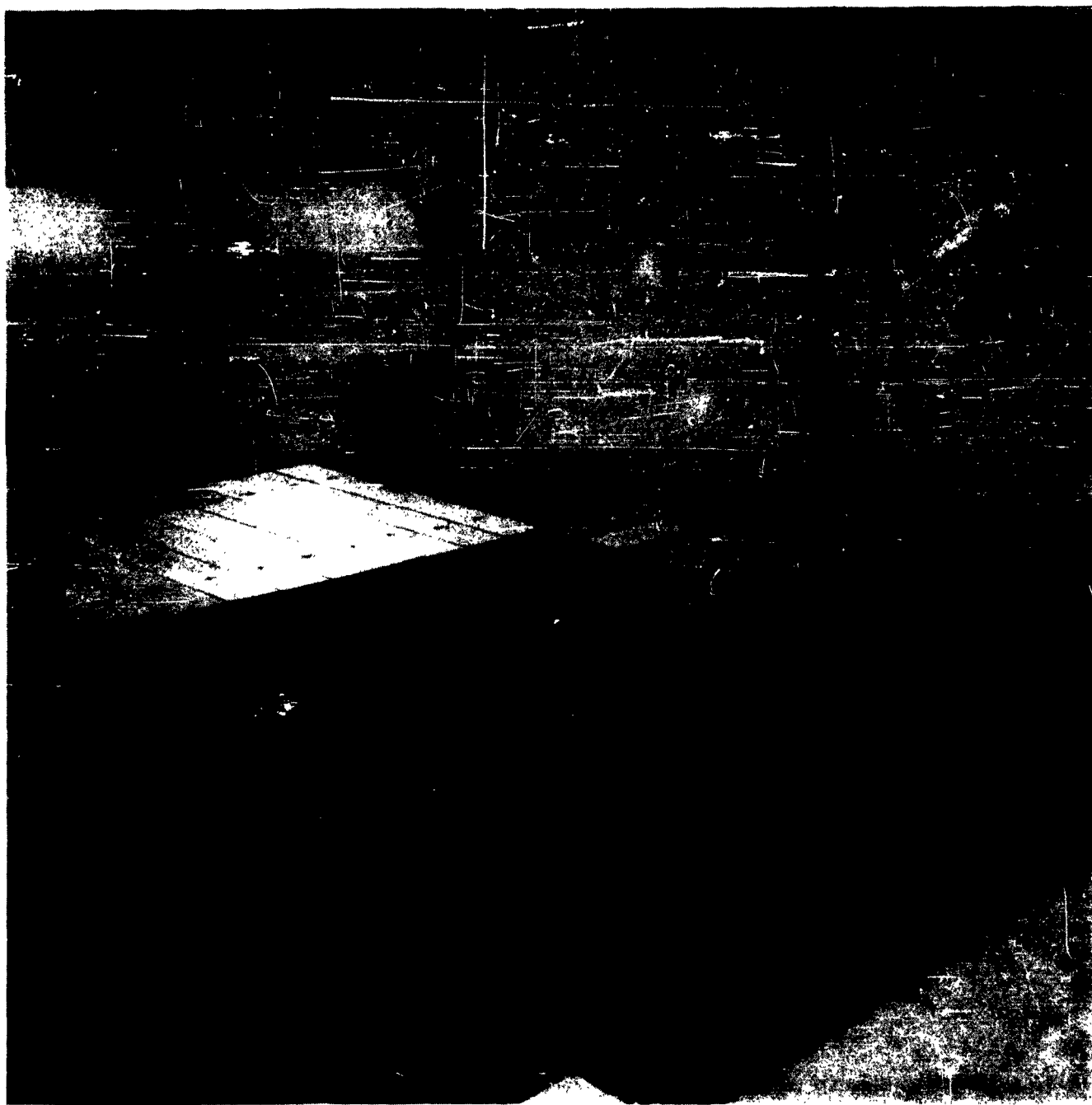
Fig. 14 - CONCRETE ENTRANCEWAY WITH ROOF SECTION REMOVED.

Fig. 15 - ASSEMBLED CONCRETE ENTRANCEWAY.

B. **Gamma Ray Measurements**

1. **Detectors**

Gamma ray dose measurements are made using the Landsverk Roentgen Meter Model L-64. This set of intercalibrated ionization chambers is capable of measuring gamma dose from a fraction of a milliroentgen to one thousand roentgens. The chambers have been intercalibrated by the manufacturer according to techniques laid down by the Bureau of Standards. The manufacturer claims a precision of $\pm$ 2 ^{o}/o, and provides calibration data for correction purposes.

The chambers are mounted on ring stands and all measurements are made on the geometric centerline of the entranceway. Sufficient care is taken in positioning the detectors and correcting for calibration and background so that the reported dose rates are accurate to better than $\pm$ 10 ^{o}/o.

2. **Sources**

The gamma sources used were point sources of Co^{60} (3.67 curies) and Cs^{137} (1.52 curies). The exact calibration procedure is described later. The Co^{60} source was held in a cylindrical brass container (1 in. o.d. x 8 in. long) which resided in a lead pig when the source was not being used. The cylinder cover was attached to heavy string which then passed through a series of eyelets fastened to the roof of the entranceway. The source was moved to the geometric center of the entranceway by operating the string at a safe distance from the source. The source was accurately positioned by sighting on a second string mounted horizontally across the entranceway at a height midway between the floor and ceiling.

The Cs^{137} source is encapsulated on the end of a brass rod of 3/16 in. diameter and 14 in. length. This rod is fitted with heavy string and is positioned in the same way as the Co^{60} source.

3. Results

Gamma measurements of dose rate in lead and concrete entranceways are summarized in the tables and figures to follow. The data is presented in such a way as to be more or less self explanatory. Position numbers are used as a handy means of identifying where a measurement was made. (Figure 16.) Distance along the centerline measures the straight line distance between source and detector. Use of the dose attenuation factor always defines the ratio of dose rate at position No. 6 (center of right angle bend) to the dose rate at position No. 1 (center of the exit plant). Note that this attenuation ratio is meaningless without the ratio ℓ_1/δ being specified.

The data of Table II is for measurements with a point source of Cs^{137} gamma rays in an 8×8 square inch cross sectional lead duct with 4 inch thick walls and one right angle bend (see Fig. 10).

Table III summarizes the measurements with a point source of Co^{60} gamma rays in the same lead duct.
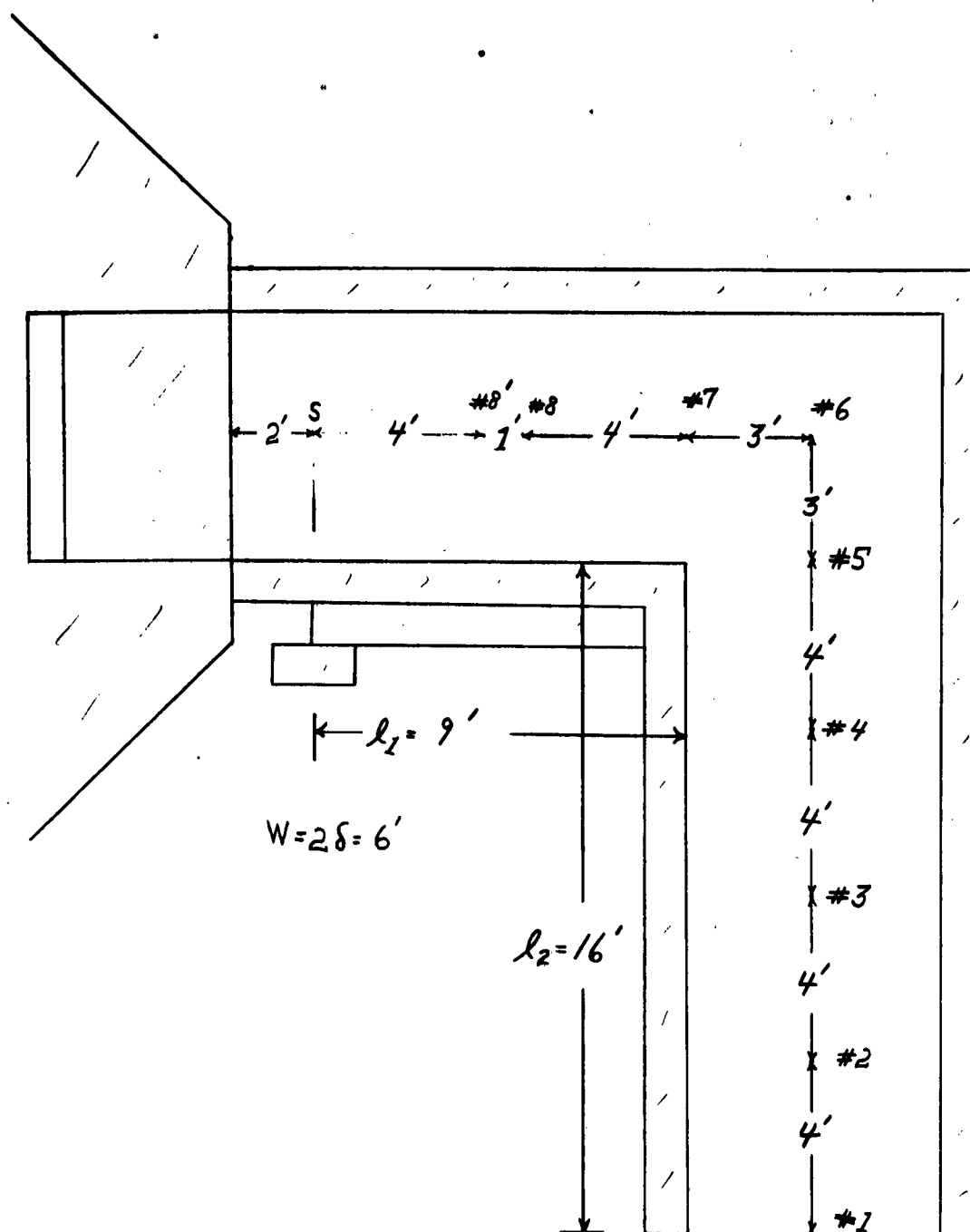
Fig. 16. GAMMA RAY MEASUREMENT POSITIONS

TABLE II

POINT SOURCE* - Cs^{137} GAMMA RAY MEASUREMENTS

IN 8" x 8" LEAD DUCT WITH 4" WALLS

Position Number	Centerline distance from source (inches)	ℓ_1 (inches)	ℓ_2 (inches)	Gamma Dose Rate mr/min	Dose attenuation factor
6	20	16	0	36.58	- - - -
1	40	16	16	0.0537	680

* 1.52 curies source.

TABLE III

POINT SOURCE*# - Co^{60} GAMMA RAY MEASUREMENTS

IN 8" x 8" LEAD DUCT WITH 4" WALLS

Position Number	Centerline distance from source (inches)	ℓ_1 (inches)	ℓ_2 (inches)	Gamma Dose Rate mr/min	Dose attenuation factor
6	20	16	0	331.3	- - - -
1	40	16	16	0.766	432

#* 3.67 curie source.

The dose attenuation factor is observed to be some 36 $^{\circ}$/o smaller for Co^{60}. This appears explainable on the basis that at Co^{60} energies the compton scattering is the dominating process while for Cs^{137} energy the photoelectric absorption process shares about equally with compton scattering.

Table IV summarizes the measured data for a point source of Cs^{137} gamma rays in a 6 by 6 foot square cross sectional concrete entrance-way with one (1) foot thick walls (see Figs. 10 through 14).

Table V summarizes the measured data for a point source of Co^{60} gamma rays in a 6 by 6 foot square cross sectional concrete entrance-way with one (1) foot thick walls.

Referring to Tables IV and V we note in comparing the dose attenuation ratios in concrete we have

Source	ℓ_1 (feet)	ℓ_2 (feet)	Dose attenuation ratio
Cs^{137}	9	16	266
Co^{60}	9	16	424

where from Tables II and III in lead we found

Source	ℓ_1 (inches)	ℓ_2 (inches)	Dose attenuation ratio
Cs^{137}	16	16	680
Co^{60}	16	16	432

TABLE IV

POINT SOURCE*, Cs^{137} GAMMA RAY DOSE MEASUREMENTS

IN 6' x 6' CONCRETE ENTRANCEWAY WITH 1' WALLS

Position Number	Centerline distance from source (feet)	ℓ_1 (feet)	ℓ_2 (feet)	Dose Rate mr/min	Dose attenuation factor
8	5	9	0	4.06	----
6	12	9	0	0.818	----
4	19	9	4	0.0401	20.4
3	23	9	8	0.01193	68.5
1	31	9	16	0.00307	266

*1.52 curie source

54

TABLE V

POINT SOURCE*, Co^{60} GAMMA RAY DOSE MEASUREMENTS

IN 6' x 6' CONCRETE ENTRANCEWAY WITH 1' WALLS

Position Number	Centerline distance from source (feet)	ℓ_1 (feet)	ℓ_2 (feet)	Dose Rate mr/min	Dose attenuation factor
7	5	5	0	33.96	-----
6	8	5	0	12.19	-----
5	11	5	0	11.16	-----
4	15	5	4	0.6223	19.5
3	19	5	8	0.1965	62.1
2	23	5	12	0.0793	154
1	27	5	16	0.0403	302
7	7	7	0	17.76	-----
6	10	7	0	7.713	-----
5	13	7	0	7.759	-----
4	17	7	4	0.3660	21.1
3	21	7	8	0.1216	63.4
2	25	7	12	0.04557	169
1	29	7	16	0.02311	334
8	4	9	0	53.4	-----
7	9	9	0	9.21	-----
6	12	9	0	6.62	-----
5	15	9	0	5.77	-----
4	19	9	4	0.256	25.9
3	23	9	8	0.0761	87.0
2	27	9	12	0.0298	222
1	31	9	16	0.0156	424

*3.67 curie source.

We thus observe the interesting fact that the ratios have reversed, Co^{60} attenuation being larger than Cs^{137} in concrete but smaller in lead. If we observe a plot of the compton and photoelectric cross section for concrete we find that both for Cs^{137} and Co^{60} the compton process alone acts, with Co^{60} having a small scattering cross section and hence a greater attenuation in the entranceway.

The lower third of the data in Table V is plotted as Fig. 17. The solid line represents a rigorous albedo calculation including corner effect. The dashed line shows the fraction of the total which is due to the scattered ·component. The circled points are measured. In general the agreement between calculation and measurement is rather good. Once the right angle bend is passed the difference between scattered and total is due to the corner effect contribution. It is not clear why the calculations show a trend to turn upward at position No. 1 (31 feet from source), resulting in a disagreement with measurement of approximately $46\ ^{o}/o$.

Table VI summarizes the calculated data for the 6' x 6' concrete entranceway with a Co^{60} point source. These data may be compared with the data in the lower third of Table V (ℓ_1 = 9 feet). Note, that the calculated (376) vs the measured (424) dose attenuation ratios are different by approximately $11\ ^{o}/o$. Reference to Fig. 17 shows why. At the 31 foot position (No. 1) the discrepancy between calculation and measurement is $46\ ^{o}/o$. Note that no normalizing of data is done. Dose calculations are absolute.

TABLE VI

POINT SOURCE*, Co^{60}, GAMMA RAY DOSE CALCULATIONS

IN 6' x 6' CONCRETE ENTRANCEWAY WITH 1' WALLS

Position Number	Centerline distance from source (feet)	ℓ_1 (feet)	ℓ_2 (feet)	Scattered dose rate (mr/min)	Direct dose rate (mr/min)	Corner effect dose rate (mr/min)	Total dose rate (mr/min)	Dose Attenuation Ratio
8	4	9	0	5.35	54.340	-------	59.695	-----
7	9	9	0	2.48	10.723	-------	13.203	-----
6	12	9	0	1.54	6.032	-------	7.572	-----
5	15	9	0	1.22	5.677	-------	6.893	-----
4	19	9	4	0.178	-----	0.0596	0.2382	31.8
3	23	9	8	0.0663	-----	0.0040	0.0703	108
2	27	9	12	0.0347	-----	0.0007	0.03546	214
1	31	9	16	0.0120	-----	0.0002	0.02017	376

*3.67 curies.

- 57 -

Fig. 17. Comparison of Calculated and Measured Co-60 Gamma Ray Dose Distribution in 6' x 6' Concrete Entranceway

point source - 3.67 curies

⊙ Total Dose Rate (Measured)

___ Total Dose Rate (Calculated)

--- Scattered Dose Rate (Calc.)

$\frac{\ell}{\delta} = 3$

$\frac{mr}{min}$

Centerline Distance from Source (ft)
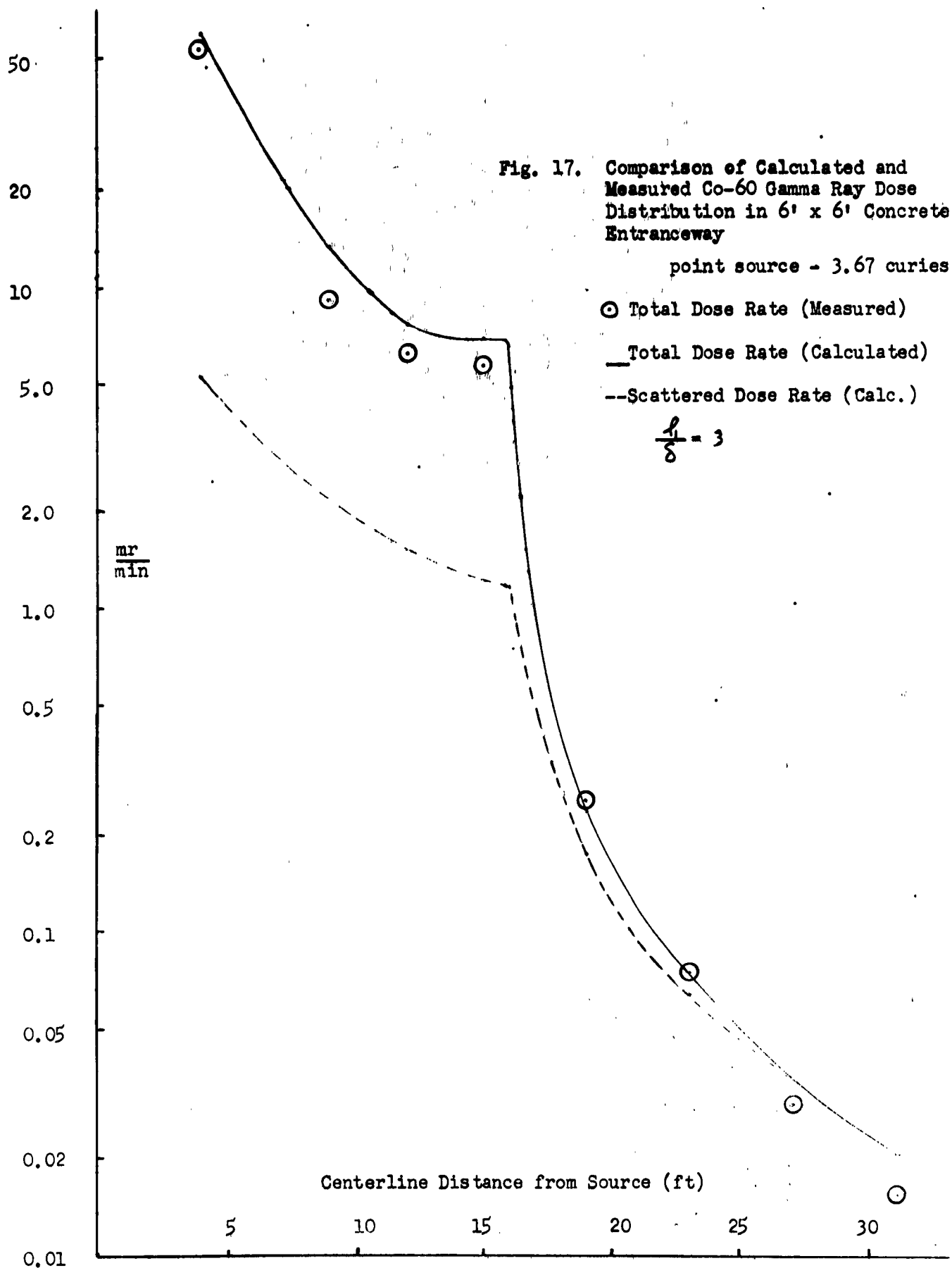
The calculated gamma dose rate has three components; direct, for those positions which see the source, scattered, at all positions and corner effect contributions which decreases as leg ℓ_2 lengthens. Note that at position No. 4 (ℓ_2 = 4 feet) the corner effect contribution (0.0596 mr/min) is 25 °/o of the total (0.2382 mr/min).

Referring to Fig. 18., for Cs^{137}, at position No. 1 almost no discrepancy exists between measurement and calculation. The measured data is taken from Table IV and the calculated results are by rigorous albedo theory including corner effect. Note, that in both Fig. 17 and Fig. 18, the calculated direct dose in leg ℓ_1 is higher than measured. This may be due to an error in source strength calibration. The calibration was done inside the reactor room where scattering off walls would give a higher indicated source strength.

In order to verify the expected effect of a radiation trap the entire roof section over the right angle bend is removed as shown in Fig. 14. The experimental data is presented in Table VII and plotted in Fig. 19.

The effect of the trap may be seen by comparing the appropriate data of Table V and VII. From Table V, without a trap, the dose attenuation ratio is 424 while with the trap the ratio is 517. The roof section contributes about equally with the floor and side wall to the scattered radiation because the angle of the incident radiation is the same and near 90°. For the rear scattering surface the incidence is perpendicular (zero degrees) and contributes less to the scattered radiation than either of the other three surfaces.

Fig. 18 Comparison of Calculated
and Measured Cs-137 Gamma Ray
Dose Distribution in 6' x 6'
Concrete Entranceway

point source - 1.52 curies

⊙ Total Dose Rate (measured)

___ Total Dose Rate (calculated)

-- Reflected Dose Rate (calc.)

$$\frac{\ell_1}{\delta} = 3$$

Centerline Distance from Source (ft)
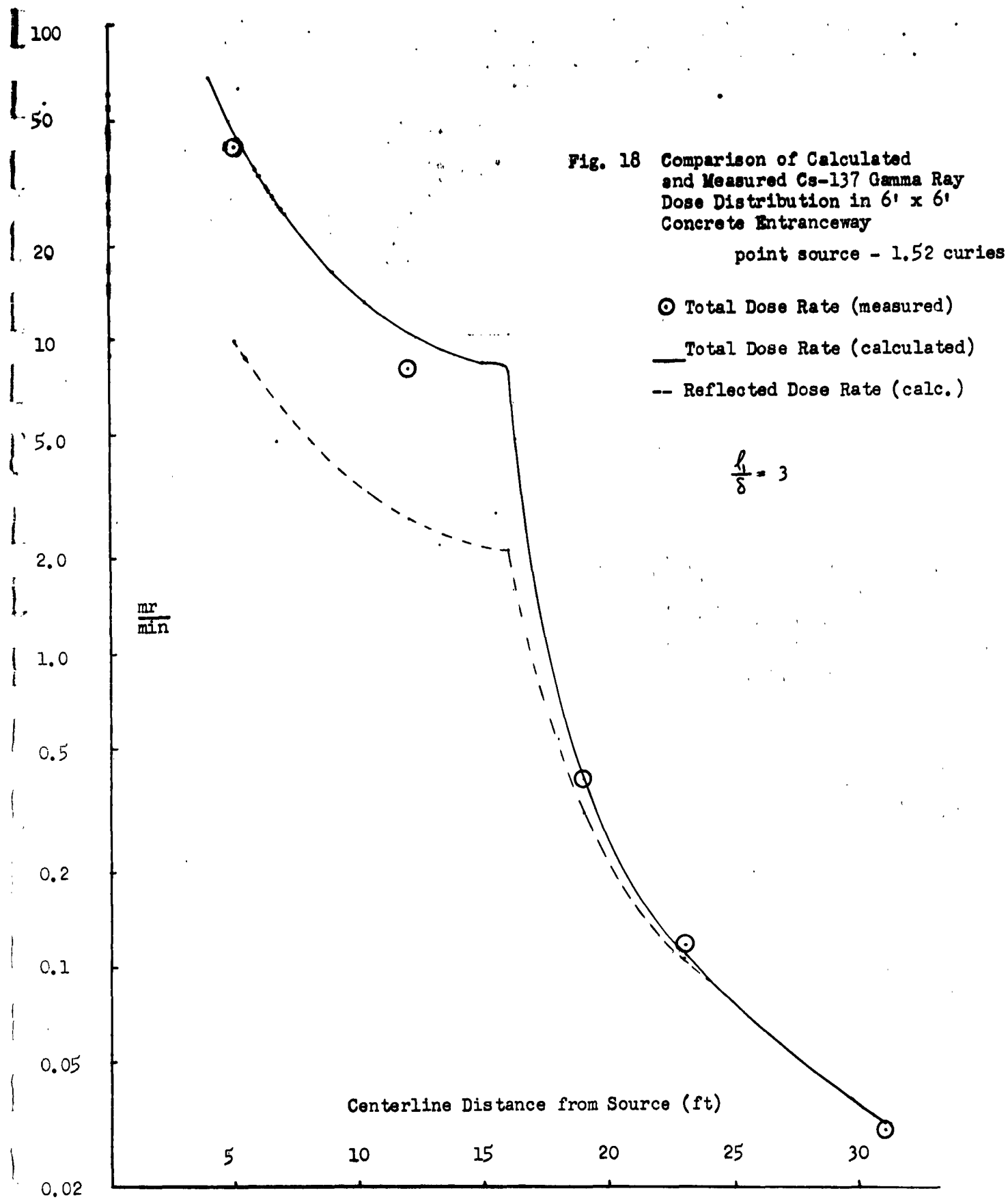
$\frac{mr}{min}$

TABLE VII

POINT SOURCE - Co^{60}# GAMMA RAY DOSE MEASUREMENTS

IN 6' x 6' CONCRETE ENTRANCEWAY WITH 1' WALLS AND WITH TRAP

Position Number	Centerline distance from source (feet)	1 (feet)	2 (feet)	Dose Rate mr/min	Dose attenuation factor
8	4	9	0	51.9	-----
7	9	9	0	10.38	-----
6	12	9	0	6.61	-----
4	19	9	4	0.212	31.1
3	23	9	8	0.0574	115
1	31	9	16	0.0128	517

#3.67 curie source

Fig. 19. Comparison of Calculated and Measured Co-60 Gamma Ray Dose Distribution in 6' x 6' Concrete Entranceway WITH TRAP

point source - 3.67 curies

⊙ Total Dose Rate (measured)

___ Total Dose Rate (calculated)

---Reflected Dose Rate (calc.)

$$\frac{\ell}{\delta} = 3$$

$\frac{mr}{min}$

Centerline Distance from Source (ft)
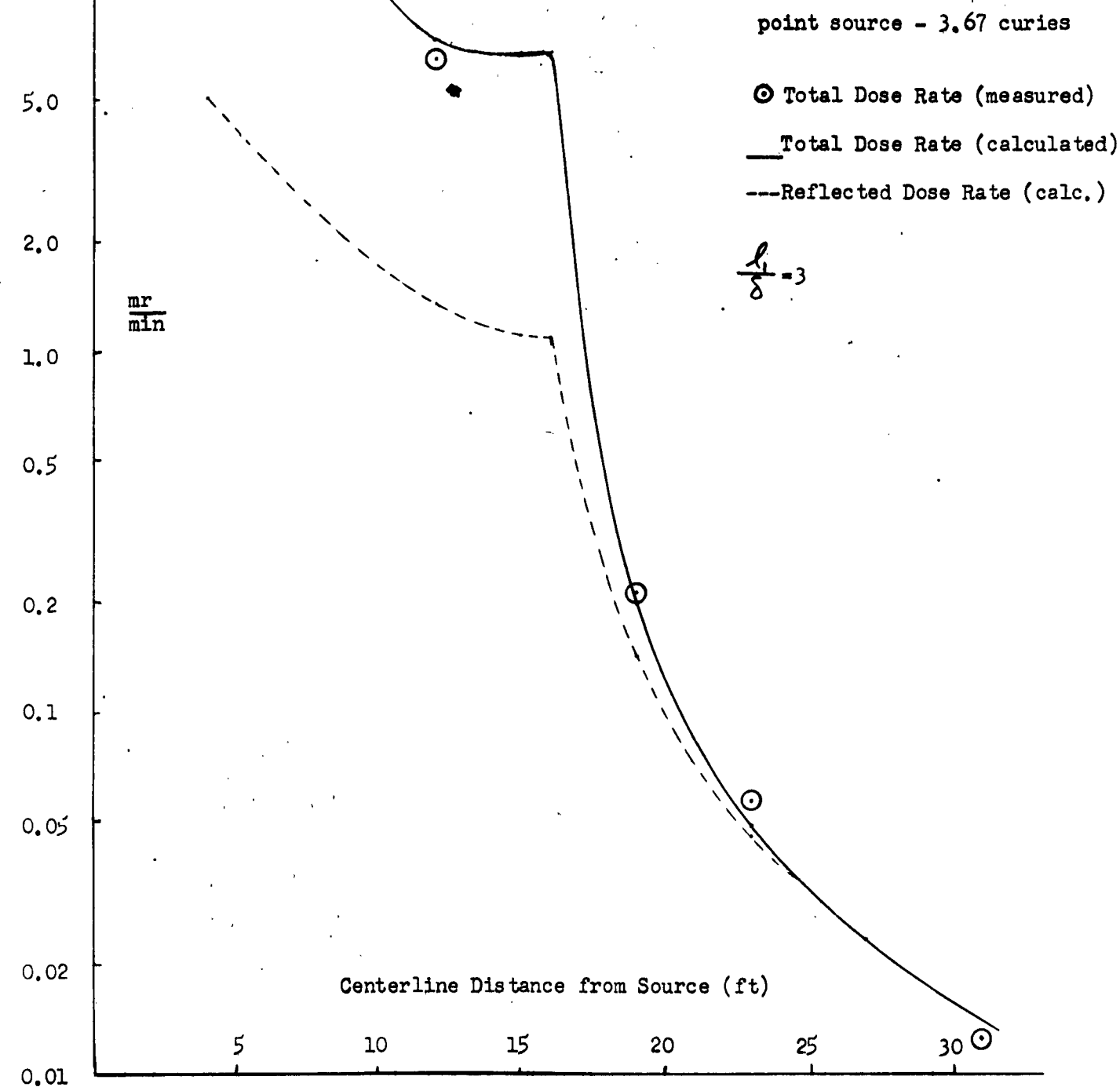
This lack of equal contribution to the scattered radiation going down leg ℓ_2 is more evidence of the angular dependency of the albedo. Comparison of Figs. 17 and 19 indicates the overall effect of the trap. The results of the trap data necessitated reconsideration of earlier ideas in which it was planned to place various thicknesses of lead on the wall immediately at the bend. It was argued that a small thickness of lead sheet on the four walls would greatly increase the attenuation of the right angle duct because of the much lower lead albedo. The lead would also reduce the corner effect materially. This is planned for future measurements.

C. Neutron Number Albedo Measurements

In order to analytically describe neutron number flux and neutron number attenuation ratios in the 6' x 6' concrete entranceway, it is desirable to again resort to albedo theory because of the success this receipt provides in describing the gamma dose distribution. Unfortunately, only the neutron dose albedos of Strickler and Hungerford are available, and these are in rather serious disagreement. (See section II-B).

To obtain a neutron number albedo, the following two measurements are made: A PuBe source and a long BF_3 counter are mounted on 12 foot poles separated by six feet out in a field. An average of twenty readings results in a count rate of 54 counts per minute. Air scattering is ignored for the 6 foot separation of source and detector.

The same source and detector are now positioned 6 feet apart
and on the axis of the leg ℓ_2 of the concrete entranceway. The position of
the counter is vertical in both measurements. We obtain a count rate of 458
counts per minute. As we have the same direct flux as outside the difference
458 - 54 = 404 is due to neutrons scattered from the walls. We now must
relate these two measurements to the neutron number albedo.

Let ϕ_o be the direct flux and ϕ_s the scattered flux. The ratio
between the in duct and free air measurements is

$$\bar{P} = 1 + \frac{\phi_s}{\phi_o} \tag{39}$$

If the source and detector is identical in both measurements and if the counter
is insensitive to the energy degradation of the scattered flux, (assumed) P is
the count rate ratio $\frac{458}{54}$ = 8.48. From previous discussion and albedo theory

$$\phi_o = \frac{N_o}{4\pi R_o^2} \tag{40}$$

where R_o is the source-detector separation and N_o is the source strength in
neutrons per second.

$$\phi_s = \frac{\alpha'}{1-\alpha'} \frac{N_o}{16\pi^2} \int_S \frac{\cos\phi \, dA}{R_1^2 R_2^2} \tag{41}$$

which is from equation 28 except that the albedo α' is here assumed to be independent of energy and angle. R_1 is the distance from source to each wall incremental scattering area and R_2 is distance from wall scattering area to detector.

Forming the ratio of (40) and (41) we obtain

$$\frac{\Phi_s}{\Phi_0} = \frac{R_0^2}{4\pi} \cdot \frac{\alpha'}{1-\alpha'} \int_S \frac{\cos\varphi \, dA}{R_1^2 \, R_2^2} \tag{42}$$

The integration is performed numerically as described in the sample calculation of section III-C-3 with the results

$$\frac{\Phi_s}{\Phi_0} = 3.60 \frac{\alpha'}{1-\alpha'} \tag{43}$$

Hence, from equation (39)

$$\bar{P} = 1 + \frac{\Phi_s}{\Phi_0} = 1 + 3.60 \frac{\alpha'}{1-\alpha'} = 8.48$$
$$\alpha' = 0.675$$

This value for the neutron number albedo is used in all calculations to follow.

D. Neutron Number Flux Measurements

1. Detectors

Ideally, as for the gamma rays, a measurement of neutron dose distribution in an entranceway is desired. To our knowledge no accurate tissue equivalent neutron dose counter is commercially available. As this program lacked sufficient funds to develop and build such a counter an attempt was made to borrow suitable instruments from ANL and ORNL without success. We thus resorted to the long BF_3 counter, which consists of a BF_3 counter surrounded by one inch of a paraffin with an outer cover of cadmium. Neutrons with energies below the cadmium cutoff of 1.44 ev are prevented from being counted.

Neutrons of energy greater than 1.44 ev in energy pass through the cadmium, are moderated in the paraffin and detected by the n,α reaction in the BF_3 counter. The overall detector assembly measures eight inches in length by three inches in diameter. The active volume of the BF_3 tube is 4-1/2 inches in length by 1 inch in diameter. While the energy response is unknown, such long counters characteristically have a somewhat uniform sensitivity to neutrons from a few mev to the resonance region. Suitable amplifier bias removes the normally small gamma sensitivity.

It should be mentioned that use of a 5 curie PuBe source results in fluxes in the 6' x 6' concrete entranceway which are too small for

foil threshold detectors or tissue equivalent ionization chambers. Scintillation crystals for accurate neutron dose measurements are unavailable commercially. Certain mixtures of ZnS and lucite are known to produce tissue equivalent doses but are beyond the scope of this program to date.

The proton recoil counter developed by Hurst and associates at ORNL are now available commercially and will be used for future neutron dose measurements.

2. Sources

An investigation of possible neutron sources for use in entranceway measurements resulted in the selection of PuBe as a practical source. Consideration was given to the use of fission plates to produce both a fission gamma and neutron spectra but were discarded because of the inordinate amount of time required for fabrication. Design of a suitable plate for future use has been completed. This plate requires cooling and will produce approximately 10^{10} neutrons/sec.

The PuBe spectrum emits neutrons ranging in energy from $\sim$ 0.1 to 12 mev with an average energy of approximately 4.5 mev. This is above the fission average of approximately 2 mev and well below the 14 mev fusion energy. As variation in dose rate with neutron energy is not large in the 1 to 10 mev range, the source appears to be a suitable substitute for both fission and fusion.

A 5 curie PuBe source was procured from ANL on loan and is convertible to a point thermal source by emersion in a 12 inch paraffin cylinder.

3. Results

The small lead ducts were not of practical size for neutron measurements. Very small sources are required and thick walls to reduce to zero, fast neutron penetration of walls. All neutrons measurements are made in the 6' by 6' concrete entranceway. Because of its very low gamma emission and average neutron energy in the range of interest, PuBe is chosen as the source. Only point source measurements have been made to date through a number of other sources are possible in future work.

PuBe point source neutron data is summarized in Table VIII and plotted in Figure 21. For convenience, the positions in which measurements are made may be located on Figure 20. for all neutron measurements.

Referring again to Fig. 21, the solid line is for the calculated neutron number flux distribution in the 6' x 6' concrete entranceway. The circled points, connected by a dotted line, are for measured points. The calculated distribution is determined by albedo theory including multiple reflections and corner effect.

As with the gamma ray measurements, neutron measurements are made at the indicated positions, with the entire entranceway, i.e.,

TABLE VIII

PuBe* NEUTRON NUMBER FLUX MEASURED DISTRIBUTION

IN 6' x 6' CONCRETE ENTRANCEWAY

Position Number	Centerline distance from source (feet)	ℓ_1 (feet)	ℓ_2 (feet)	C/min	Flux** n/cm^2-sec	mrem/hr***	number attenuation ratio
1	31	9	16	52	2.82	0.414	26.1
1a	30	9	15	60	3.25	0.478	22.6
2	27	9	12	102	5.52	0.812	13.3
2a	24	9	9	152	8.23	1.21	8.90
3a	21	9	6	268	14.5	2.13	5.05
4a	18	9	3	502	27.2	4.00	2.69
4b	17	9	2	625	33.8	4.97	2.17
4c	16	9	1	813	44.1	6.48	1.66
5	15	9	0	1071	57.9	8.52	1.26
6	12	9	0	1353	73.2	10.8	----
7	9	9	0	1990	108	15.9	----
8a	6	9	0	3159	171	25.2	----
9a	3	9	0	5499	298	43.8	----

* S = 7.09 x 10⁶ n/sec

** 312 C/min = 16.9 n/cm^2-sec

*** 6.8 n/cm^2-sec = 1 mrem/hr.
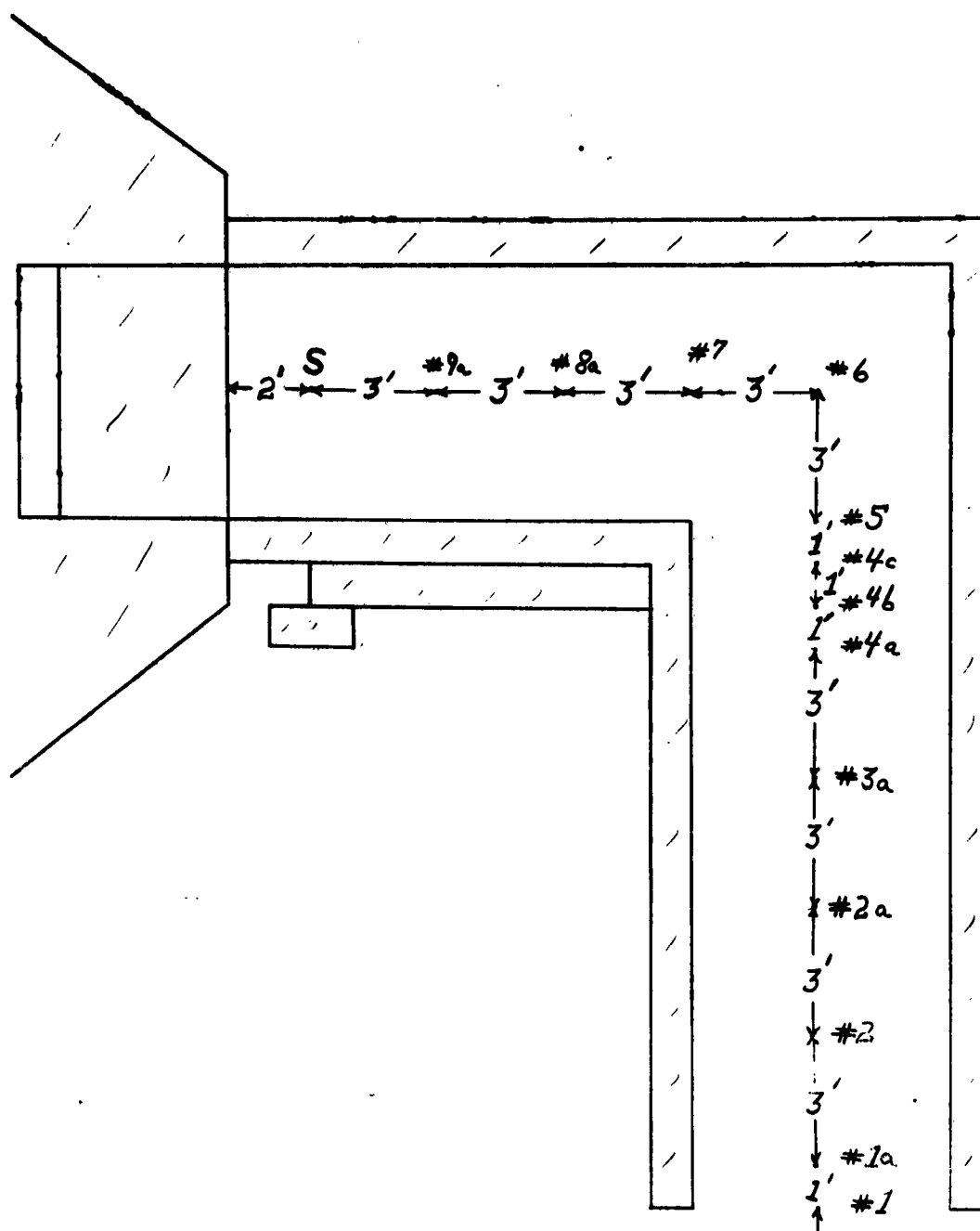
Fig. 20. NEUTRON NUMBER FLUX MEASUREMENT POSITIONS
IN 6' x 6' CONCRETE ENTRANCEWAY

Fig. 21. PuBe Neutron Number Flux Distribution in 6' x 6' Concrete Entranceway

$\alpha' = 0.675$

⊙ measured dose point

___ calculated dose

$l/s = 3$

$\emptyset$
n/cm^2-sec

Centerline Distance from Source (ft)
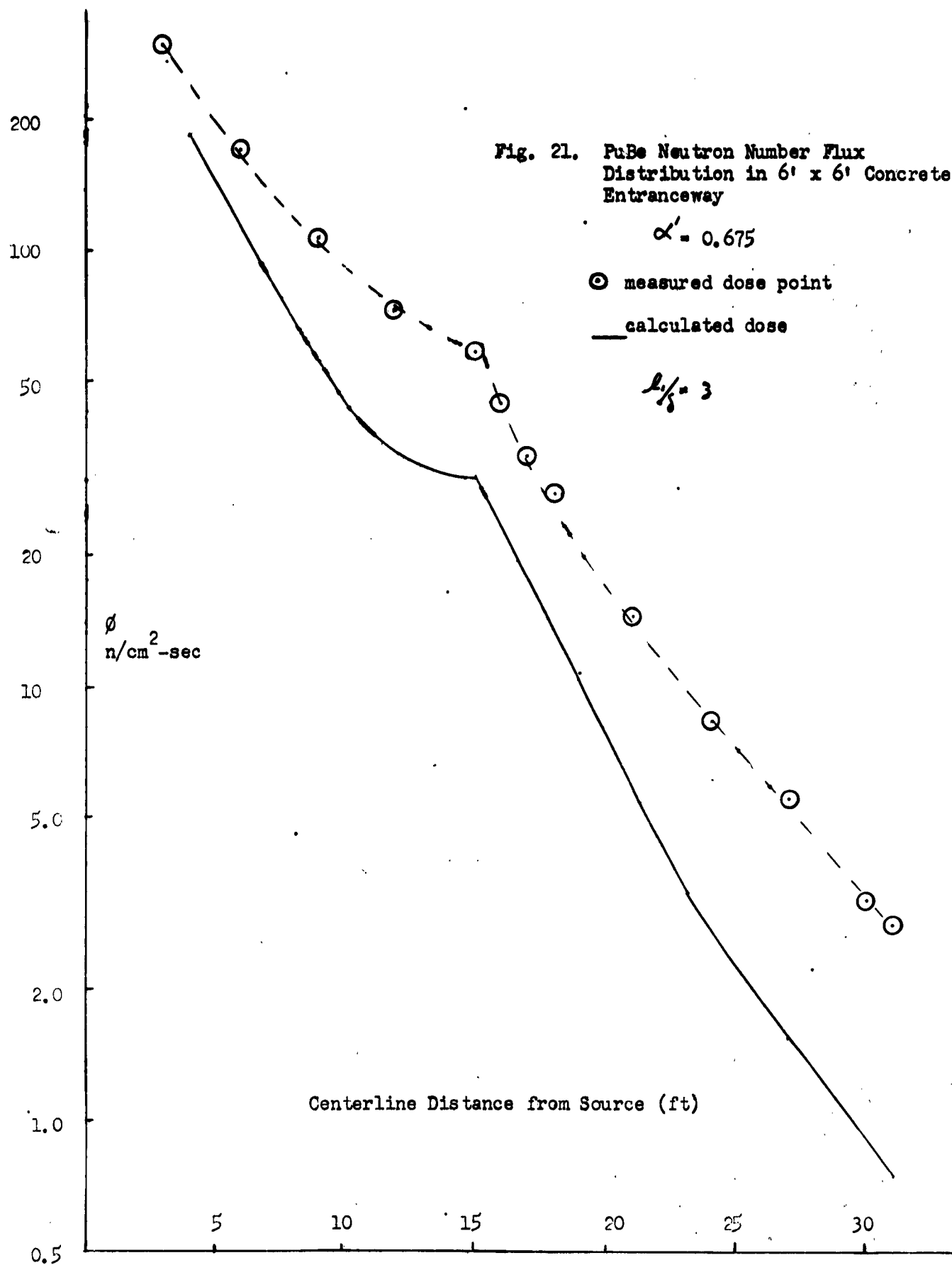
ℓ_2 = 16' feet always present. Hence, Table VIII indicates an ℓ_2 length as
if the measurement is made with that position at the end of ℓ_2. The presence
of more wall scattering area behind the measurement position certainly adds
some small contribution. The conversion factors indicated at the bottom
of Table VIII are derived in a later section of this report.

Table IX presents the calculated data plotted in Fig. 21.
Comparison of calculated vs measured neutron number attenuation ratio is
seen from Tables VIII and IX (position No. 1) to be 43.7 calculated and 26.1
measured for an ℓ_2 of 16 feet with ℓ_1/δ = 3. We suspect the measurement
for a number of reasons. Assuming the number flux falls of as we have measured
and calculated, it is important to emphasize that the dose distribution would
fall of considerably faster. The neutrons at the exit end of the entranceway
are degraded in energy and therefore deliver less dose. The small number
attenuation ratios are never-the-less worthy of some concern for shelter
designers and future experiments should measure a neutron dose distribution,
tissue equivalent if possible.

The effect of a trap is again investigated by removing the roof
section over the right angle bend in the 6' x 6' concrete entranceway. The
data are presented in Table X and plotted in Fig. 22.

A comparison of the neutron number attenuation ratios of Tables
VIII and X indicates almost a negligible difference. The roof scattering
surface and hence by symmetry the floor surface makes a very small contribution
to the number flux at the exit. This is surprising as we have had other indi-
cations that the angular dependence of the neutron number albedo is small.
This evidence is to the contrary.

TABLE IX

CALCULATED PuBe* NEUTRON NUMBER FLUX DISTRIBUTION

IN 6' x 6' CONCRETE ENTRANCEWAY

Position Number	Centerline distance to source (feet)	ℓ_1 (feet)	ℓ_2 (feet)	Direct flux (n/cm^2-sec)	Scattered flux (n/cm^2-sec)	Corner effect flux (n/cm^2-sec)	Total flux (n/cm^2-sec)	Number Attenuation Ratio
1	31	9	16	0	0.770	0.0055	0.775	43.7
2	27	9	12	0	1.516	0.045	1.56	21.7
3	23	9	8	0	3.253	0.068	3.32	10.2
4	19	9	4	0	9.910	0.715	10.63	3.17
5	15	9	0	3.95	26.2	0	30.10	1.12
6	12	9	0	4.19	29.5	0	33.80	----
7	9	9	0	7.47	48.3	0	55.75	----
8	4	9	0	40.3	144	0	184.3	----

*Source = 7.09 x 10^6 n/sec

Fig. 22. PuBe Neutron Number Flux
Distribution in 6' x 6' Concrete
Entranceway WITH TRAP

Source = 7.09×10^6 n/sec

⊙ measured dose point

—— calculated dose

$$\frac{\ell}{\delta} = 3$$

ϕ
n/cm^2-sec

Centerline Distance from Source (ft)
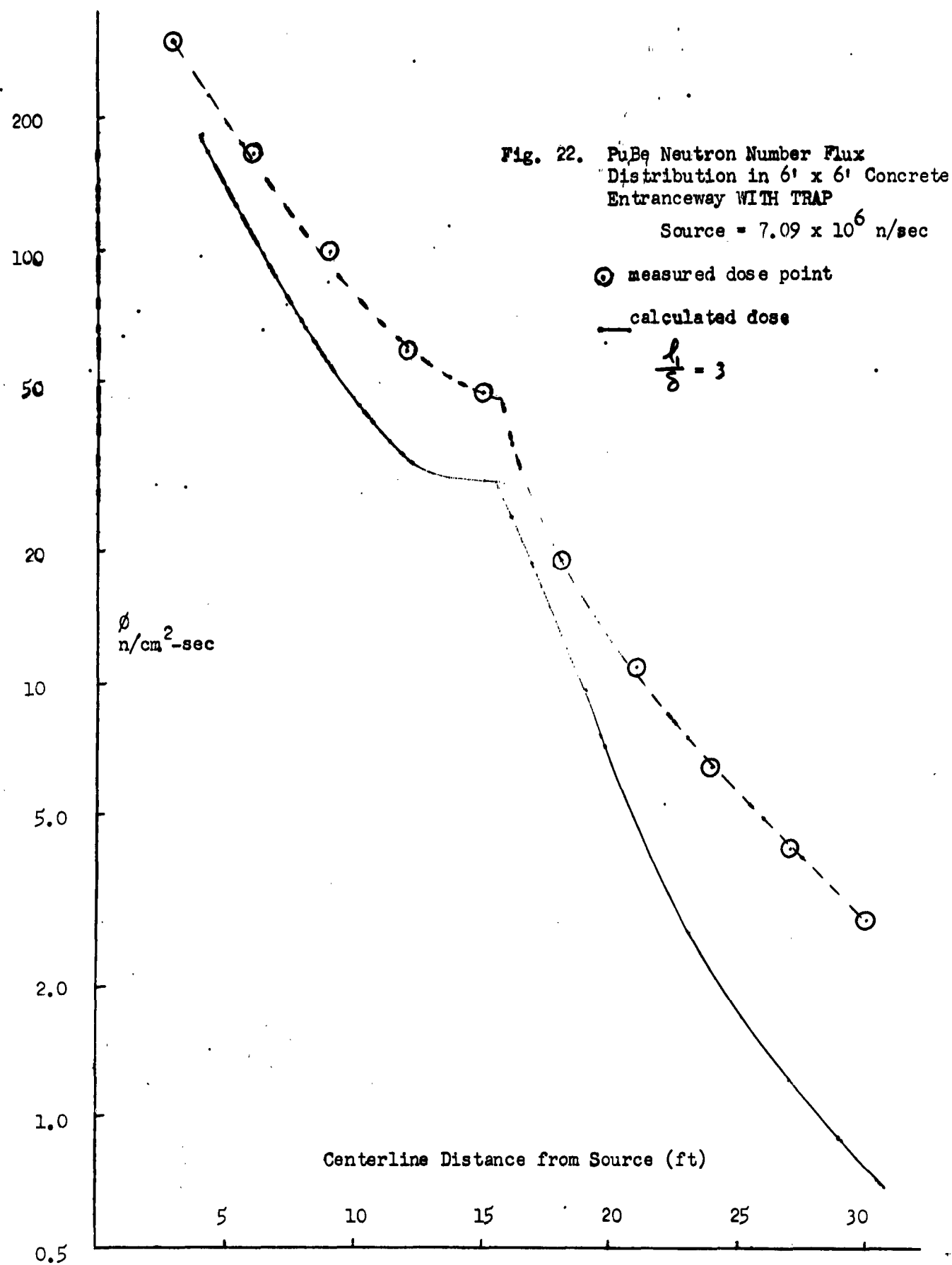
TABLE X

MEASURED PuBe* NEUTRON NUMBER FLUX DISTRIBUTION

IN 6' × 6' CONCRETE ENTRANCEWAY WITH TRAP

Position Number	Centerline distance from source (feet)	ℓ_1 (feet)	ℓ_2 (feet)	C/min	Flux** n/cm^2-sec	Number Attenuation Ratio
1	31	9	16	----	-----	-----
1a	30	9	15	54	2.93	20.0
2	27	9	12	77	4.17	14.0
2a	24	9	9	120	6.48	9.05
3a	21	9	6	203	11.0	5.33
4a	18	9	3	356	19.3	3.04
5	15	9	0	867	47.1	1.24
6	12	9	0	1082	58.6	-----
7	9	9	0	1811	98	-----
8a	6	9	0	3055	165	-----
9a	3	9	0	5533	300	-----

*Source = 7.09×10^6 n/sec

**16.9 n/cm^2-sec = 312 C/min.

In an attempt to get some information about the energy spectra of the neutron distribution in the concrete entranceway, a series of thermal neutron measurements are made. Table XI presents data for a PuBe point source and thermal neutron distribution measurements. The data is plotted in Fig. 23. The PuBe source is immersed in paraffin sufficiently thick to thermalize all neutrons. With this thermal source, replacing the PuBe spectrum source, another thermal neutron distribution measurement is made. These data are given in Table XII and plotted on Fig. 23.

From Fig. 23, two points of interest are evident. First, the thermal number flux attenuation ratio is distrubingly small ($\sim$ 15 from Table XII). Recall the PuBe number flux attenuation ratio was also small ($\sim$ 43.7 from Table IX).

Second, the thermal flux distribution from the PuBe source falls off with a very similar slope to the thermal flux distribution from the thermal source. One might suspect that as we proceed down the entranceway the number of thermals would increase because of thermalization effects.

Little more can be learned from the thermal flux data. Apparently the flux thermalizes significantly early in leg ℓ_1. Hence, again a dose distribution is needed and would show, based on these results that the dose attenuation ratio is far larger than the measured number flux attenuation ratio.

TABLE XI

MEASURED THERMAL NEUTRON NUMBER FLUX DISTRIBUTION

IN 6' x 6' CONCRETE ENTRANCEWAY WITH PuBe SOURCE

Position Number	Centerline distance to source (feet)	ℓ_1 (feet)	ℓ_2 (feet)	Counts/min	Number attenuation ratio
1	31	9	16	-----	------
1a	30	9	15	145	10.52
2	27	9	12	235	6.49
2a	24	9	9	352	4.33
3a	21	9	6	485	3.15
4a	18	9	3	820	1.86
5	15	9	0	1244	-----
6	12	9	0	1527	-----
7	9	9	0	1910	-----
8a	6	9	0	2647	-----
9a	3	9	0	3390	-----

*Source = 7.09×10^6 n/sec.

- 77 -

TABLE XII

MEASURED THERMAL NEUTRON NUMBER FLUX DISTRIBUTION

IN 6' x 6' CONCRETE ENTRANCEWAY WITH THERMAL NEUTRON SOURCE

Position Number	Centerline distance from source (feet)	ℓ_1 (feet)	ℓ_2 (feet)	Counts per minute	Number attenuation ratio
1	31	9	16	- - - -	- - - -
1a	30	9	15	85	14.5
2	27	9	12	147	8.38
2a	24	9	9	232	5.31
3a	21	9	6	372	3.31
4a	18	9	3	559	2.21
5	15	9	0	990	- - - -
6	12	9	0	1233	- - - -
7	9	9	0	1826	- - - -
8a	6	9	0	2761	- - - -
9a	3	9	0	4497	- - - -

Fig. 23. Measured Thermal Neutron Number Flux Distribution in 6' x 6' Concrete Entranceway

$$\frac{\ell}{\delta} = 3$$

PuBe Source

Thermal Source

C/min

Centerline Distance from Source (ft)
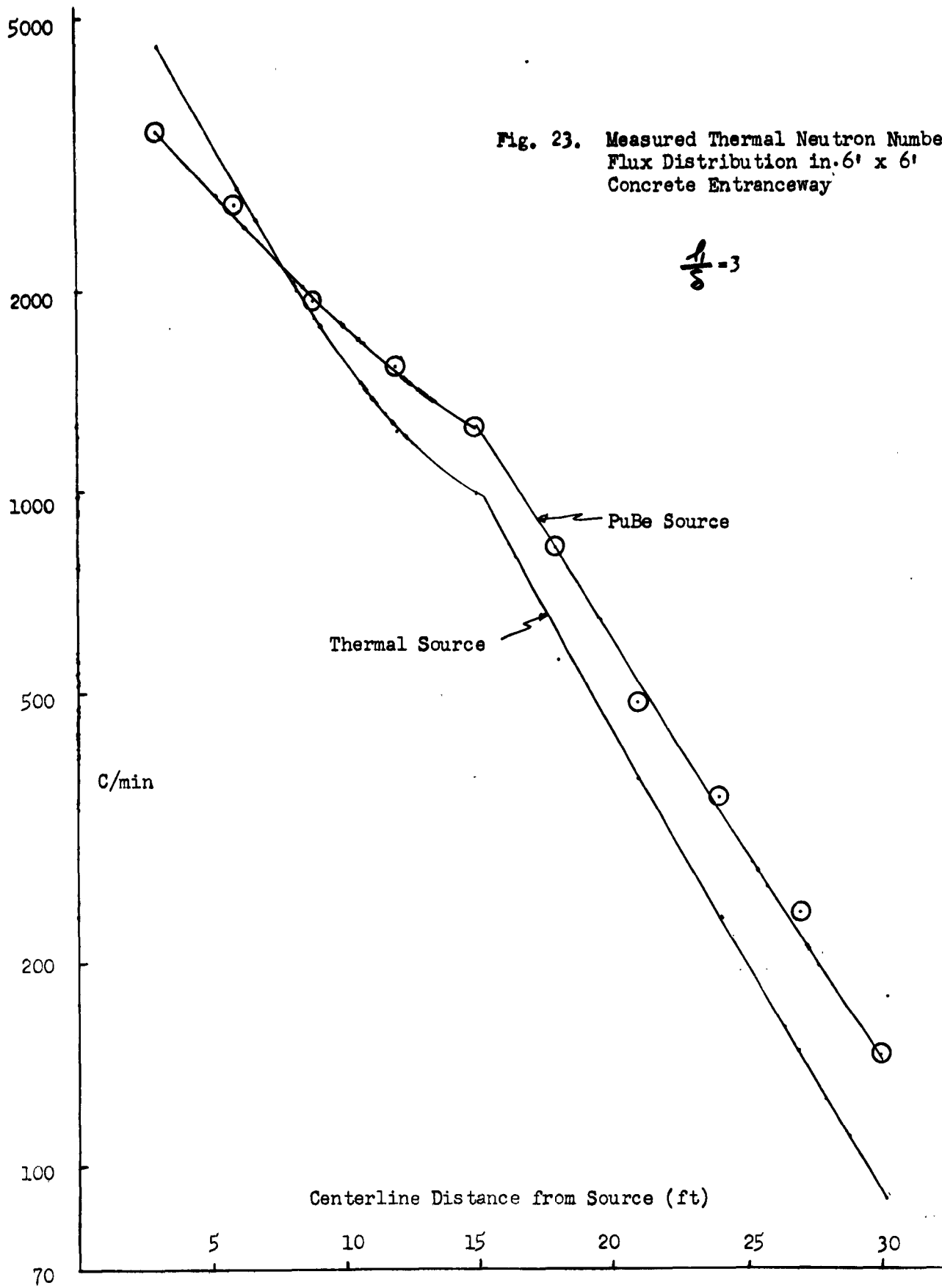
V.   SOURCE CALIBRATION PROCEDURE

Aside from a comparison of calculated vs measured attenuation ratios in the ducts it is desirable to compare on an absolute basis the calculated vs measured dose distributions.   The precision of the Landsverk's chambers makes this feasible but of questionable value in the case of neutrons measured with a long BF_3.

A. Gamma Source

The source and detectors are places as far as possible from any scattering surfaces.   Detector readings are taken at various distances from the source.   The results are plotted in Fig. 24. for both Cs^{137} and Co^{60}.
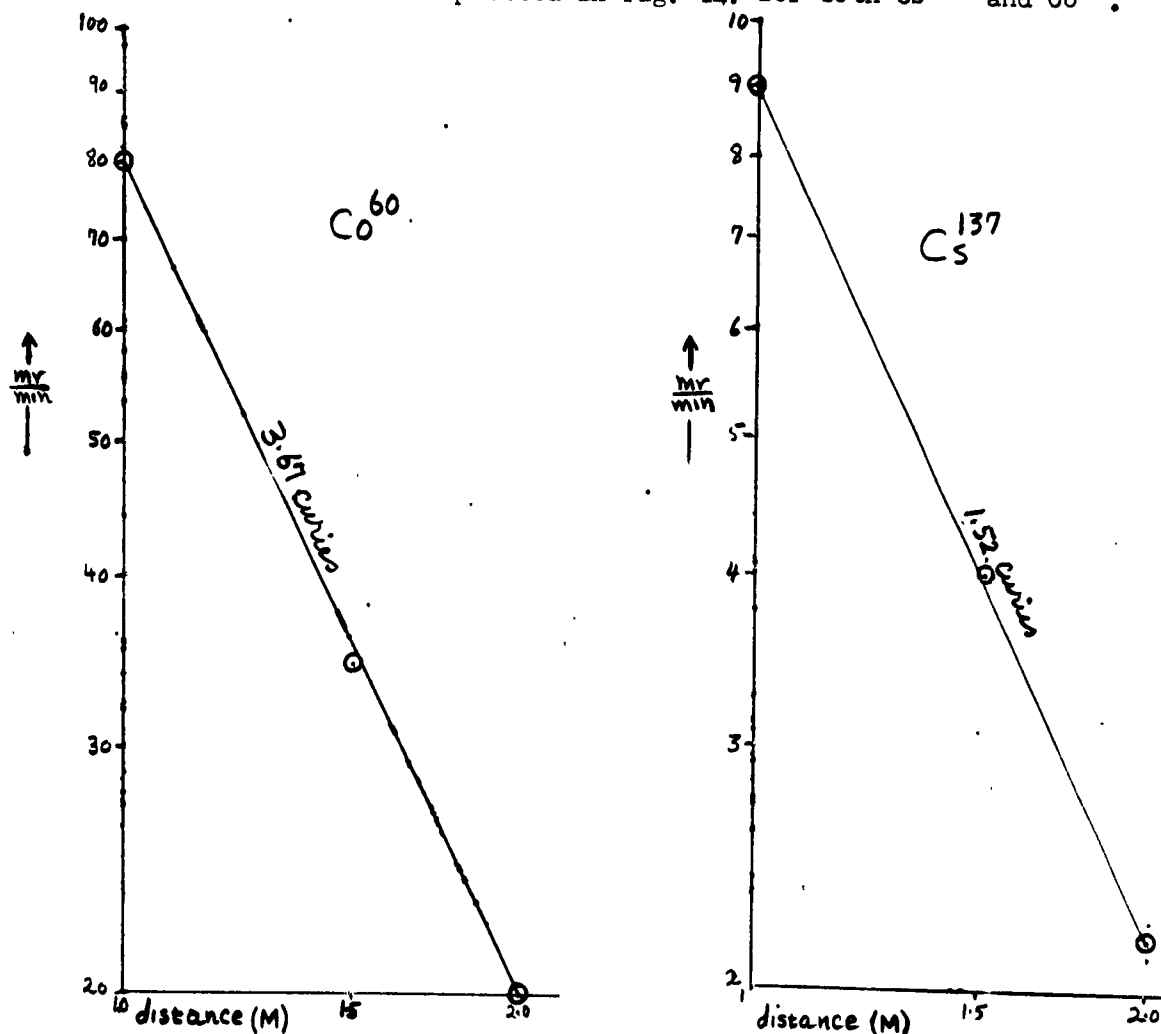

Fig. 24.   Gamma Source Strength Calibration Determination

Using the conversion factor 1.32 R/hr[12] per curie at 1 meter for Co^{60} and 0.356 R/hr per curie at 1 meter for Cs^{137} we find

Source	Curies
Co^{60}	3.67
Cs^{137}	1.52

(1 curie = 3.7 x 10^{10} dis/sec.)

B. Neutron Sources

The PuBe neutron source is calibrated by Mound Laboratory as to its neutron emission rate. The value is

$$7.09 \times 10^6 \text{ n/sec.} \sim 5 \text{ curies}$$

For distances in which air scattering is negligible, the conversion from source strength to mrem/hr may be made as follows, at 6 feet:

$$\emptyset = \frac{S}{4\pi R^2} = \frac{7.09 \times 10^6}{4\pi (6 \times 12 \times 2.54)^2} = 16.9 \text{ n/cm}^2\text{-sec}$$

From the N. B. S. Handbook No. 63, the flux equivalent to 1 mrem/hr, F(E), at all energies in the PuBe spectrum is found and plotted. An average value of F(n/cm^2-sec per mrem/hr) is obtained by numerical integration of the PuBe energy flux distribution[13] and the F(E) function.

---

[12] Radiological Health Handbook, U. S. Sept. of Health, Education and Welfare (Jan. 1957).

[13] Stewart, L. Phys. Rev. 98 (1955).

$$F = \frac{\int \emptyset(E) \, F(E) \, dE}{\int \emptyset(E) \, dE}$$

We find

$$6.8 \text{ n/cm}^2\text{-sec} = 1 \text{ mrem/hr}$$

for PuBe.

Hence, at a distance of six feet in air we have

$$\frac{16.9}{6.8} = 2.49 \text{ mrem/hr.}$$

As stated previously, in the neutron albedo measurement, we have detector readings at six feet. The results are summarized below:

Source (Curies)	Yield (n/sec)	Flux (6 feet) (n/cm^2-sec)	Dose (6 feet) mrem/hr	Detector reading C/min.	C/min per mrem/hr
~5	7.09×10^6	16.90	2.49	312	126

VI. SUMMARY AND CONCLUSIONS

The material reported herein describes a series of analytical and experimental efforts directed toward the determination of neutron and gamma ray distributions in ducts and entranceways. By ground rule agreement, integral transport theory and Monte Carlo methods are excluded from use on

this program. The albedo receipt is applied but with considerable modification and rigor. The agreement of the albedo model and experiment is rather good for gamma rays and rather poor for neutrons.

The orientation of the program is such that full scale personnel shelter concrete entranceways are emphasized. A 6' x 6' concrete entranceway with 1 foot thick walls is constructed with a single right angle bend but with provision for a second bend. Lead ducts are also used.

Gamma dose distributions are calculated and measured in both lead and concrete ducts. Agreement between calculation and measurement is good.

Neutron number flux distributions are calculated and measured with considerably less agreement. The results of the flux measurements clearly show that neutron dose measurements must be made. Such measurements are now possible and with considerable accuracy through use of the Stanrad Neutron Dose Detector.

The need for a major dose albedo experimental effort for neutrons and gamma rays is of paramount importance. This laboratory is planning such a program in conjunction with further entranceway streaming measurements. Specific recommendations for additional entranceway studies are contained in a proposal submitted concurrently with this report.

Appendix I

on

LIST OF ADDITIONAL REFERENCES

Appendix I

LIST OF ADDITIONAL REFERENCES

1. Barcus, J. R., TID-4500 (14th Ed.) SCTM21-59(16), "Transmission of Neutrons by Cylindrical Ducts Penetrating Radiation Shields", (March 1959).

2. Berger, M. J. and Raso, D. J., NBS Report 5982, "Backscattering of Gamma Rays", (July 1958).

3. Clare, A. B., AERE-R2924, "The Measurement of Neutron Dose", United Kingdom Atomic Energy Authority Research Group Report, (1959).

4. Cure, J. W. and Hurst, G. S., "Fast Neutron Scattering: A Correction for Dosimetry", Nucleonics, Aug. 1954, pp. 36-38.

5. Davison, B., Neutron Transport Theory, Int. Series of Monographs on Physics, Oxford University Press; London (1957).

6. Eisenhauer, C. M. to LeDoux, J. C., personal communication.

7. Fisher, Edward, "The Streaming of Neutrons in Shields", Nu. Sci. and Engr. 1, pp. 222-238 (1956).

8. Glass, F. M. and Hurst, G. S., "A Method of Pulse Integration Using the Binary Scaling Unit", Rev. of Sci. Inst. 23, No. 2, pp. 67-72, (Feb. 1952).

9. Goldstein, Herbert, Fundamental Aspects of Reactor Shielding, Addison-Wesley Pub. Co., Inc., Reading, Mass. (1959).

10. Holt, J. R. and Litherland, A. E., "A Fast Neutron Spectrometer", Rev. of Sci. Instr. 25, 298 (1954).

11. Hornyak, W. F., "A Fast Neutron Detector", Rev. of Sci. Inst., Vol. 23, No. 6 (June 1952).

12. Hungerford, H. E., "Some Ground Scattering Experiments Performed at the Bulk Shielding Facility", CF-52-4-99-Now Unclassified, Apr. 1952.

13. Hurst, G. S., Ritchie, R. H., and Wilson, H. N., "A Count-Rate Method of Measuring Fast Neutron Tissue Dose", Rev. of Sci. Instr. 22, 981 (1951).

14. Hurst, G. S., and Wagner, E. B., "Special Counting Techniques in Mixed Radiation Dosimetry", Sym. on Selected Topics in Radiation Dosimetry, Vienna, Austria.

15. Johnson, D. W. and Romesberg, E. J., KAPL-2007 "Calculation of Flux to Dose Rate Conversion Factors for Fast and Intermediate Energy Neutrons".

16. Kinsman, S., ed. Radiological Health Handbook, U. S. Dept. of Health, Ed. and Welfare, Jan. 1957.

17. LeDoux, Technical Report 025, Project Y-F011-05-329, "Nuclear Radiation Shielding Provided by Buried Shelters."

18. LeDoux Technical Note N-381, Proj. Y-F011-05-329, "Analysis of the Critical Shielding Volume for Underground Shelters."

19. LeDoux, J. C., to Eisenhauer, C. M., personal communication.

20. LeDoux, J. C., and Chilton, A. B., "Attenuation of Gamma Radiation Through Rectangular Ducts and Shelter Entranceways-An Analytical Approach", NCEL Technical Note N-383.

21. Patterson, H. W., Hess, W. N., Moyer, B. J., and Wallace, R. W., "The Flux and Spectrum of Cosmic-Ray Produced Neutrons as a Function of Altitude", Health Physics, Vol. 2, pp. 69-72 (1958).

22. Peebles, G. H., R-240, "Gamma-Ray Transmission Through Finite Slabs", (Dec. 1, 1952).

23. Perkins, J. F., "Monte Carlo Calculation of Gamma-Ray Albedos of Concrete and Aluminum", Jour. of App. Phy., Vol. 26, No. 6, pp. 655-658 (June 1955).

24. Price, W. J., Nuclear Radiation Detection, McGraw-Hill Book Co., Inc. New York (1958).

25. Ritchie, R. H., "Calculations of Energy Loss Under the Bias in Fast Neutron Dosimetry", Health Physics, Vol. 2, pp. 73-76 (1958).

26. Rockwell, T. ed., "Reactor Shielding Design Manual", TID-7004 (1956).

27. Roe, G. M., KAPL-712, "The Penetration Neutrons Through an Empty Cylindrical Duct in a Shield".

28. Rossi, H. H., and Failla, G., "Tissue-Equivalent Ionization Chambers," Nucleonics 14, (2) 32 (1956).

29. Simon, A. and Clifford, C. E., CF-52-6-165 Now Unclassified, "Phenomenological Theory of the Attenuation of Neutrons by Air Ducts in Shields," (June 1952).

30. Simon, A. and Clifford, C. E., "The Attenuation of Neutrons by Air Ducts in Shields", Nu. Sci. and Engr. 1, 156-166 (1956).

31. Shore, F. J. and Schamberger, R. D., BNL 390 (T-74), "The Transmission of Neutrons Through Ducts in Water", (March 1, 1956).

32. Spencer, L. V., and Hubbell, J. H., NBS-Report 5659, "Report on Current Knowledge of Shielding From Nuclear Explosions".

33. Stephenson, R., Introduction to Nuclear Engineering, McGraw-Hill Book Co., Inc. New York (1958).

34. Strickler, T. D., Gilbert, H. E., and Auxier, J. A., "Fast Neutron Scattering from Thick Slabs", Nu. Sci. and Engr. 3, 11-18 (1957).

35. Tarks, L., KAPL-201, "Leakage of Neutrons Past a Step in an Annulus."

36. Thompson, B. W., UCRL-2748, "Portable Fast and Slow-Neutron Survey Meter" (1954).

37. Vortman, L. J. (Director), WT-1218 (Feb-May 1955), "Operation Teapot-Evaluation of Various Types of Personnel Shelters Exposed to an Atomic Explosion."

38. Wagner, E. B., and Hurst, G. S., "Advances in the Standard Proportional Counter Method of Fast Neutron Dosimetry", Rev. of Sci. Inst. Vol. 29, No. 2, pp. 153-158 (Feb. 1958).

39. Wagner, E. B. and Hurst, G. S., "Gamma Response and Energy Loss in the Absolute Fast Neutron Dosimeter", Health Physics, Vol. 2, pp. 57-61 (1959).

40. Wilf, H. to Terrell, C. W., personal communication.

41. Whitcombe, D. W., AFCD-3413, "A Diffusion Solution for the Cylindrical Ducting Problem of Infinite Geometry."

42. Young, D. S., LA-1938, "Paraffin Cylinders to Measure Neutron Energies".

Appendix II

on

THE APPROXIMATE ALBEDO APPROACH IN ANALYTICAL FORM

Appendix II

THE APPROXIMATE ALBEDO APPROACH IN ANALYTICAL FORM[14]

The work presented in this appendix is a summary of a short but rather accurate method to the solution of the square cross section duct problem. The method holds well over a range of length to width ratios of 1 or 2 up. Neither the exit angle or the angle between the entrance and exit planes is taken into account in the plots of albedos on page 32 because of the lack of information. This approach gives the angles to use when this information becomes available. The approach is broken down into three contributions:

1. Albedo Wall Scatter

$$A_{wss} \text{(area of wall seen by source)} = (2\,\delta_1)\frac{(\ell_1 + 2\,\delta_2)}{\ell_1}H$$

$$A_{wsd} \text{(area of wall seen by detector)} = (2\,\delta_2)\frac{(\ell_2 + 2\,\delta_1)}{\ell_2}H$$

where:

ℓ_1, ℓ_2 refer to the lengths of legs 1 and 2 respectively,

H is the height, and

δ_1, δ_2 = half-width of legs 1 and 2 respectively.

---

[14] Originally in Contract Report No. 8 (June 21, 1960) of Contract NBy-3185 (U).

Fig. 25.   APPROXIMATE ALBEDO GEOMETRY

Areas A_{dtw} and A_{stw} are A_{wsd} and A_{was} plus the additional
"effective area" caused by penetration of the corner. Although penetration
is not uniform, the total effect is an increase in the directly seen area. The
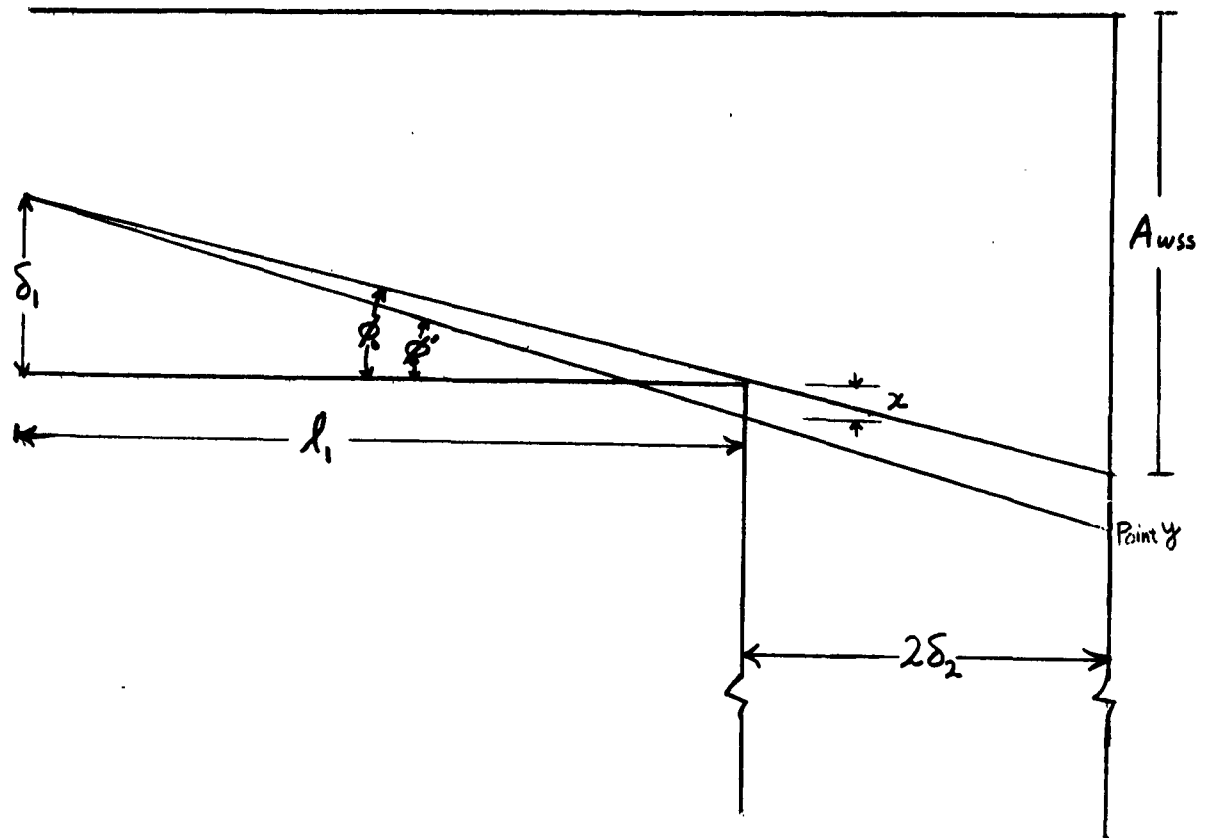geometry is:

Fig. 26. Corner Penetration Geometry

The dose at point y is:

$$D_y = \text{(dose at y without corner)} \; e^{-\mu_o(x/\sin\phi_o')}$$

where μ_o is the attenuation coefficient (neutron or gamma) of the corner material

-89-

and ϕ_o' is the angle from the source to the corner relative to the wall of the duct; and is actually the penetration angle. Since the dose decreases very rapidly with an increase in x, the effective added width of the tunnel x_{os} (Fig. 25.) is quite small and $\phi_o' \cong \phi_o$. Thus the total dose imparted to the wall (after multiplying by the similar triangle relation $(\dfrac{l_1 + 2\delta_2}{l_1})$ and height H is:

$$\text{Area x Dose}_p \cong \int_0^\infty (\frac{l_1 + 2\delta_2}{l_1}) \; H \; (\text{Dose at point y without corner}) \; e^{-\mu_o(x/\sin\phi_o)} \; dx$$

$$= (\frac{l_1 + 2\delta_2}{l_1}) \cdot H \; (D_{yo}) \int_0^\infty e^{-(\frac{\mu_o x}{\sin\phi_o})} \; dx$$

$$= (\frac{l_1 + 2\delta_2}{l_1}) \; H \; (D_{yo}) \; \frac{\sin\phi_o}{\mu_o}$$

Considering D_{yo} to be approximately the same as the average dose to the total wall surface A_{wss}, we have

$$A_{stw}(\text{total area seen by source}) = A_{wss} + \frac{(\sin\phi_o) \; H \; (l_1 + 2\delta_2)}{l_1\mu_o}$$

$$A_{stw} = A_{wss} \left[1 + \frac{\sin\phi_o}{2 \; \delta_1\mu_o} \right]$$

Similarly:

$$A_{dwt}(\text{total area seen by detector}) = A_{wsd} + \frac{(\sin \phi_1) \, H \, (\ell_2 + 2 \delta_1)}{\mu \, \ell_2}$$

$$A_{dtw} = A_{wsd} \left[1 + \frac{\sin \phi_1}{2 \; \delta_2 \mu} \right]$$

where ϕ_0 and ϕ_1 are the average angles to the corner from the source and detector points respectively, and μ_0 and μ are the attenuation coefficients for the incident and scattered radiation respectively.

These angles ϕ_0 and ϕ_1 are closely given by:

$$\phi_0 = \tan^{-1} \left(\frac{\frac{\sqrt{5}}{2} \delta_1}{\ell_1}\right) \quad \text{and} \quad \phi_1 = \tan^{-1} \left(\frac{\frac{\sqrt{5}}{2} \delta_2}{\ell_2}\right).$$

As a rule of thumb - the scattered radiation has an energy of the original scattered radiation after going through a 90° bend (down to approximately 0.5 mev for gamma rays). The extra corner penetration also adds areas to the top and bottom thusly:

$$A_{stb}(\text{total area of the bottom seen by the source}) = (4 \, \delta_1 \, \delta_2)$$

$$+ 4 \, \frac{\tan \phi_0}{\mu_0 \, \ell_1} \quad (\delta_2^2 \, \ell_1 \mu_0 + \delta_2^2 + \ell_1 \, \delta_2)$$

$$A_{stb} = 4 \, \delta_1 \, \delta_2 \left[1 + \frac{\delta_2}{\delta_1} \quad \tan \phi_0 + \frac{\tan \phi_0}{\mu_0 \delta_1} \quad (1 + \frac{\delta_2}{\delta_1}) \right]$$

A_{dtt}(total area of top seen by detector) $= (4 \, \delta_1 \, \delta_2)$

$$+ \, 4 \, \frac{\tan \phi_1}{\mu \, \ell_2} \, (\, \delta_2^2 \, \ell_2 \mu + \delta_1^2 + \ell_2 \ell_1)$$

$$A_{dtt} = 4 \, \delta_1 \, \delta_2 \left[1 + \frac{\delta_1}{\delta_2} \quad \tan \phi_1 + \frac{\tan \phi_1}{\mu \, \delta_2} \quad (1 + \frac{\delta_1}{\delta_2}) \right]$$

The average reciprocal squared distance to these areas (or surfaces) is given by:

Area	Average Reciprocal Square Distance from Source $(1/R_s^2)$	Average Reciprocal Square Distance to Detector $(1/R_d^2)$
A_{stw}	$\dfrac{1}{(\ell_1 + 2 \delta_2)^2 + \frac{1}{2} \delta_1^2 + \frac{1}{8} H_2}$	$\dfrac{1}{(\ell_2 + \delta_1)^2 + \delta_2^2 + \frac{1}{8} H^2}$
A_{dtw}	$\dfrac{1}{(\ell_1 + \delta_2)^2 + \delta_1^2 + \frac{1}{8} H^2}$	$\dfrac{1}{(\ell_2 + 2 \delta_1)^2 + \frac{1}{2} \delta_2^2 + \frac{1}{8} H^2}$
A_{stb} or A_{dtt}	$\dfrac{1}{(\ell_1 + \delta_2)^2 + \frac{1}{4} H^2}$	$\dfrac{1}{(\ell_2 + \delta_1)^2 + \frac{1}{4} H^2}$

The angle Θ is the angle from the source (incident) or detector (exit) to the average point of the surface as measured from a perpendicular to that surface.
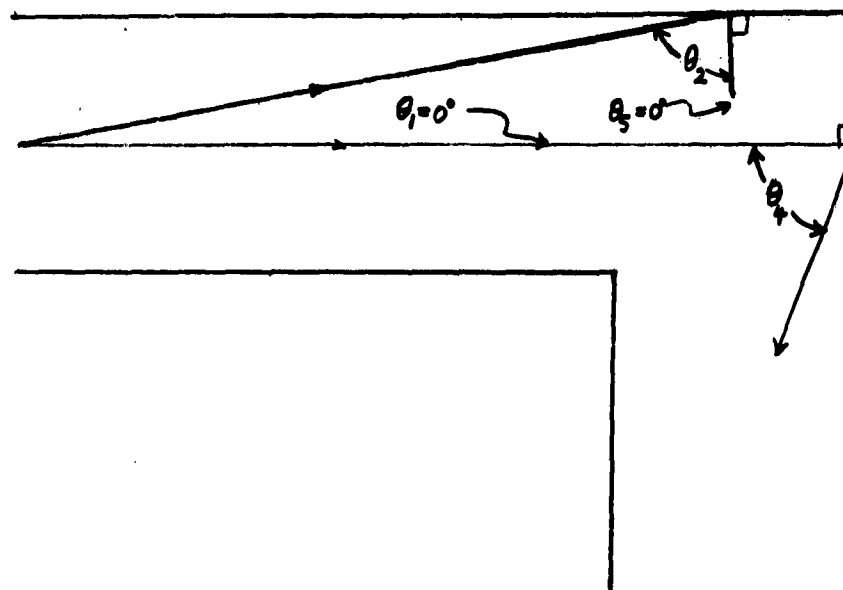
Fig. 27. Albedo Angles

The angles used in the albedos are:

Area	Angle of Incidence	Angle between Planes (if used)	Angle of Exit (if used)
A_{stw}	$\theta_1 = 0°$	$0°$	$\theta_4 = \tan^{-1}(\frac{(\ell_2 + \delta_1)}{\delta_2})$
A_{dtw}	$\theta_2 = \tan^{-1}(\frac{(\ell_1 + \delta_2)}{\delta_1})$	$0°$	$\theta_5 = 0°$
A_{stb} or A_{dtt}	$\theta_3 = \tan^{-1}(\frac{(\ell_1 + \delta_2)}{\delta_1})$	$90°$	$\theta_6 = \tan^{-1}(\frac{(\ell_2 + \delta_1)}{\delta_2})$

The final form for the albedo scattered dose is:

$$D_S = \frac{kN_o}{4\pi} \left(\frac{A_{stw}\cos\Theta_1 \, \alpha(\Theta_1, \, 0°, \, \Theta_4)}{2\pi R_s^2 R_d^2} + \frac{A_{dtw}\cos\Theta_2 \, \alpha(\Theta_2, \, 0°, \, \Theta_5)}{2\pi R_s^2 R_d^2} \right.$$

$$\left. + \frac{(A_{stb} + A_{dtt}) \cos\Theta_3 \, \alpha(\Theta_3, \, 90°, \, \Theta_6)}{2\pi R_s^2 R_d^2} \right)$$

Where k is the flux to dose conversion factor. The form with only incident angle albedo, such as those derived previously would be:

$$D_S = \frac{kN_o}{4\pi} \left(\frac{A_{stw}\cos\Theta_1 \, \alpha(\Theta_1)}{2\pi R_s^2 R_d^2} + \frac{A_{dtw}\cos\Theta_2 \, \alpha(\Theta_2)}{2\pi R_s^2 R_d^2} \right.$$

$$\left. + \frac{(A_{stb} + A_{dtt}) \cos\Theta_3 \, \alpha(\Theta_3)}{2\pi R_s^2 R_d^2} \right.$$

2. Corner Scattering Toward the Detector

Using single scattering (the differential Klein-Nishina cross section) technique (described in more detail in this report under "single scattering" section), the amount of scattered radiation that is scattered through an average angle of $90° - \phi_o - \phi_1$ is:

$$D_{ac} = \frac{N_o Hk \sin\phi_o \sin\phi_1}{4\pi r_s^2 r_d^2 \mu_o \mu} \; K(90° - \phi_o - \phi_1, E_o) \; P(90° - \phi_o, \phi_1, E_o)$$

where

-94-

$$r_s^2 = (\ell_1 + \delta_1)^2 + 3/2 \; \delta_1^2, \text{ in cm}^2$$

$$r_d^2 = (\ell_2 + \delta_2)^2 + 3/2 \; \delta_2^2, \text{ in cm}^2$$

μ_o and μ in cm^{-1}, H in cm, and

K = the Klein-Nishina differential cross section for scattering through an angle of $90° - \phi_o - \phi_1$, with the energy of the incident radiation E_o, in cm^{-1} of corner material. P is the energy degradation factor for the above angle and energy. For neutrons, the use of $\Sigma_s/4\pi$ should be sufficient for K, and P almost unity for heavy elements.

3. Direct Penetration

For small ducts, direct penetration may be a problem, however in general it is not. The dose would be

$$D_P = \frac{N_o \; ke^{-\mu_o r}}{4\pi (\ell_1 + \delta_1)^2 (\ell_2 + \delta_2)^2} \; B_d(\mu_o r)$$

r is equal to the distance traveled through the material, μ_o = total absorption coefficient (or dose attenuation coefficient for neutrons), and $B_d(\mu_o r)$ is the dose build-up factor.

The total dose is:

$$D = D_S + D_C + D_P.$$